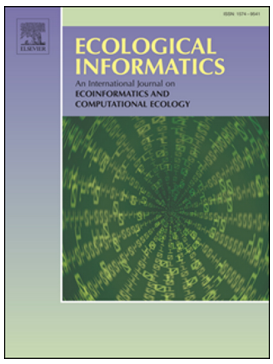

Spatio-temporal evaluation of MODIS temperature vegetation dryness index in the Middle East

Younes Khosravi, Saeid Homayouni, Taha B.M.J. Ouarda

PII: S1574-9541(24)00436-9

DOI: https://doi.org/10.1016/j.ecoinf.2024.102894

Reference: ECOINF 102894

To appear in: *Ecological Informatics*

Received date: 22 July 2024

Revised date: 11 November 2024

Accepted date: 11 November 2024

Please cite this article as: Y. Khosravi, S. Homayouni and T.B.M.J. Ouarda, Spatio-temporal evaluation of MODIS temperature vegetation dryness index in the Middle East, *Ecological Informatics* (2024), https://doi.org/10.1016/j.ecoinf.2024.102894

Spatio-Temporal Evaluation of MODIS Temperature Vegetation Dryness Index in the Middle East

Younes Khosravi[a,b,*], Saeid Homayouni[c], Taha B.M.J. Ouarda[a]

[a]Canada Research Chair in Statistical Hydro-Climatology, Institut National de la Recherche Scientifique, Centre Eau Terre Environnement, INRS-ETE, 490 de la Couronne, Québec, QC, G1K 9A9, Canada, younes.khosravi@inrs.ca, taha.ouarda@inrs.ca
[b]Environmental Science Research Laboratory, Department of Environmental Science, Faculty of Science, University of Zanjan, 45371-38791 Zanjan, Iran
[c]Centre Eau Terre Environnement, Institut National de la Recherche Scientifique (INRS), Quebec, QC, G1K 9A9 Quebec, Canada, saeid.homayouni@inrs.ca

Abstract

Drought, a recurring meteorological event, can potentially cause devastating consequences for human populations, and its attributes vary significantly across diverse geographic areas. Therefore, recognizing drought events is paramount for strategically planning and managing water resource systems. In this study, the Temperature Vegetation Dryness Index (TVDI), derived using Moderate-Resolution Imaging Spectroradiometer (MODIS) data spanning from 2003 to 2022 in the Middle East, was used as the foundation for both trend and spectral analyses. To assess TVDI trends, the Mann-Kendall test and Sen's slope estimator were utilized, and harmonic analysis was conducted for spectral analyses. These methods were applied to a dataset comprising 258,087 pixels within the specified region, covering various time scales, including monthly and seasonal analyses. The monthly analyses indicated significant growth in March and April, with September showing the least significant increase, suggesting stability or decline. Geographically, upward trends were predominant in the northern Middle East, including Turkey, Syria, Iraq, western Iran, and eastern Jordan. Significant downward trends were observed in the southern Middle East during the warmer months. Seasonal assessments showed no significant TVDI trends in winter, but upward trends in the south, west, and northwest were identified during spring. The annual trend map indicates a long-term declining trend in TVDI for most regions within specific latitudes, particularly those below 34 degrees. The results of harmonic analysis revealed the presence of multiple cycles at a 95% confidence level. Notably, there was a heightened prevalence of significant sinusoidal cycles, especially the 2-3-year cycles. This cycle was widespread in countries such as Iran, Oman, Yemen, and Turkey, as well as in the southern regions of Saudi Arabia and Egypt.

Keywords: Temperature-Vegetation Dryness Index (TVDI), Trends, Spectral Analysis, Middle East, Teleconnection, Drought.

1. Introduction

Drought has had significant spatial and temporal extents, influencing the amount, quality, and distribution of water, food availability, and the stability of natural ecosystems through various heterogeneous environmental processes (Li et al., 2019; Piao et al., 2010; Vicente-Serrano et al., 2012). This phenomenon is influenced by various factors, such as climate change, vegetation degradation, human activities, etc. (Lazzarini et al., 2015; Zhu et al., 2024). The rapid intensification of drought can significantly affect ecosystems by impositioning excessive evaporative stress on the environment (McEvoy et al., 2016; Otkin et al., 2013). Moreover, it can contribute to compound extreme events, resulting in cascading impacts, such as an elevated risk of wildfire occurrence, depletion of water resources, deterioration of air quality, and a reduction in food security (Christian et al., 2020; Gerken et al., 2018; Laz et al., 2023b; Yuan et al., 2019). Numerous recent studies have shown a clear relationship between climate change and the increasing frequency and severity of droughts around the world (Behifar et al., 2023; Dai, 2011; Trenberth et al., 2014) Large land areas have experienced physical changes in precipitation patterns and increased temperatures accompanied by a decrease in soil moisture, leading to aggravation of drought intensity (Lian et al., 2021). Severe droughts, heatwaves, sandstorms, and vegetation degradation caused by extreme weather are more frequently occurring, further negatively impacting ecological environments and human populations (Basha, Ouarda, & Marpu, 2015; Hamdi et al., 2021; Ouarda et al., 2019). Understanding how these droughts unfold in space and time is crucial for developing more effective mitigation strategies and building resilient water management practices. In this regard, the Middle East stands out as one of the regions consistently subjected to the impacts of widespread droughts (Karakani et al., 2021), primarily driven by its arid climate, high population growth, and intense agricultural activities. This situation has a profound impact on the lives of millions of individuals (Shetty, 2006).

Over the past few decades, drought assessment techniques have undergone significant evolution. Drought assessment can be achieved through contemporary remote sensing techniques or conventional climatic drought indices (Khosravi et al., 2024) . Ensuring precise and timely drought monitoring is vital in global environmental transformations (Chen et al., 2015). Numerous climate indices such as the standardized precipitation index (SPI) (McKee et al., 1993), rainfall anomaly index (RAI) (Huete et al., 1999), Palmer Drought Severity Index (PDSI) (Palmer, 1968), drought area index (DAI) (Bhalme & Mooley, 1980), Vegetation condition index (VCI) (Kogan, 1995), SEPI (Vicente-Serrano et al., 2010), effective drought index (EDI) (Ali et al., 2011; Byun & Wilhite, 1999), reconnaissance drought index (RDI) (Tsakiris et al., 2007), and soil moisture deficit index (SMDI) (Narasimhan & Srinivasan, 2005) have been proposed and widely used to monitor drought. Indices reliant on meteorological data frequently prove insufficient or

inaccessible, particularly in regions with limited weather stations or marked spatial variability (Khosravi & Abbasi, 2016; Zormand et al., 2017). This limitation has necessitated the adoption of satellite-based remote sensing techniques, which provide continuous spatial coverage, especially in areas where ground observations are sparse. Remote sensing offers valuable tools for capturing drought conditions' onset, extent, and severity (Hao et al., 2015; Mokarram & Zarei, 2023). By utilizing these data, drought processes can be monitored continuously, enabling the observation of changes over both time and space. Since 1980, various drought indices have been suggested for the monitoring of drought, utilizing remote sensing data in the visible (VIS), shortwave infrared (SWIR), near-infrared (NIR), and thermal infrared (TIR) (Chaerle & Van Der Straeten, 2000; Gerhards et al., 2019).

Currently, remote sensing data sources for drought assessment primarily encompass Landsat TM (Thematic Mapper), ETM+ (Enhanced Thematic Mapper), OLI (Operational Land Imager) (Ghaleb et al., 2015; Ozelkan et al., 2016), Sentinel SAR (Synthetic Aperture Radar), MSI (Multispectral Imager) (Puletti et al., 2019), and MODIS (Moderate Resolution Imaging Spectroradiometer) (Klisch & Atzberger, 2016; Wan et al., 2004). Landsat and Sentinel datasets boast impressive spatial resolutions (30 m and 10 m). However, their extended revisit cycles pose challenges when encompassing the entire study area. Consequently, Landsat and Sentinel data are the most effective for small-scale regional drought monitoring efforts. In contrast, MODIS exhibits a short revisit period, occurring twice daily, and features a wealth of remote sensing images with a moderate spatial resolution of 500 meters. This suits it for extensive large-scale drought monitoring research (Puletti et al., 2019). In this context, MODIS data have been widely employed to derive vegetation and temperature-based drought indices, which are crucial in capturing large-scale drought dynamics (Wei et al., 2021; Wu et al., 2015).

Remote sensing technology is instrumental in extensively monitoring drought, employing techniques classified into vegetation indices and temperature-based approaches. Nevertheless, there are constraints in using soil temperature and vegetation indices for soil moisture monitoring, stemming from factors like incomplete vegetation coverage and temporal lag. In response to this challenge, Sandholt et al. (2002) introduced the Temperature Vegetation Dryness Index (TVDI), a method founded on the interplay between vegetation and land surface temperature. Following Carlson et al. (1990), the scatter diagram depicting the relationship between NDVI (Normalized Difference Vegetation Index) and LST (Land Surface Temperature) assumes a trapezoidal shape. Sandholt et al. (2002) introduced the TVDI based on the LST-NDVI triangle model, where the warm edge is treated as a parallel line. NDVI and LST exhibit a robust correlation, typically resulting in a negative curve corresponding to the warm edge (Guo et al., 2023; Liu et al., 2018; Tang et al., 2010; Wan et al., 2021). However, Ehrlich and Lambin (1996) observed a positive relationship where

vegetation conditions evolve with surface temperature over time. This positive correlation is susceptible to shifts, particularly as seasons progress into drier months due to climate change. This dynamic could increase the uncertainty of TVDI for larger areas and higher NDVI values (Guo et al., 2023). Overall, numerous researchers (Bian et al., 2023; Li et al., 2008; Sandholt et al., 2002; Son et al., 2012; Sun et al., 2008; Wan et al., 2004; Wang et al., 2010) have employed the TVDI to evaluate surface moisture conditions and drought monitoring.

The arid and semi-arid regions of the Middle East rely heavily on fragile rain-fed or irrigated agricultural systems, making them particularly vulnerable to periodic climate fluctuations and changes in hydrological conditions (Kaniewski et al., 2012). Over the past four decades, many eastern dryland countries, including Iran, Jordan, the UAE, and Turkey, have experienced rising temperatures coupled with declining precipitation levels (Basha, Marpu, & Ouarda, 2015; Kafle & Bruins, 2009; Ouarda et al., 2014; Soltani et al., 2012; Tayanç et al., 2009). Drought periods have recurred irregularly and spatially heterogeneously, with the most severe, prolonged, and widespread events occurring in the past decade (Al-Qinna et al., 2011). Moreover, the Middle East has exceeded the water resource capacity needed to sustain its population for extended periods. In response, the region has sought to expand its water distribution and storage infrastructure, primarily through dam and canal construction. However, it faces critical challenges due to recurring droughts and declining aquifer levels (De Chatel, 2017; De Châtel, 2007; Gonzalez et al., 2016; Morris, 1997). The confluence of factors, including water scarcity (Oki & Kanae, 2006) and the recurring incidence of drought in the Middle East (Mishra & Singh, 2010), exerts a notable influence on crop yields and the regional economy (Kaniewski et al., 2012). According to the United Nations World Water Development Report, several districts in the Middle East are experiencing ‘extremely high’ water scarcity (UNESCO, 2021). These circumstances increase the risk of both human and property losses (Agrawala et al., 2001). Consequently, when assessing drought impacts, this region emerges as particularly significant due to factors such as population density, susceptibility, the severity of drought events, and the potential for increased aridity due to climate change (Barlow et al., 2016).

Exploring the spatial and temporal variations of climatic parameters provides valuable insights into understanding the dynamics influencing their time series. A comprehensive examination of trends, oscillations, and cycles governing these time series is particularly important in this context. Significant efforts have been dedicated to the analysis of drought frequency and trends in recent years, with notable contributions from Karabörk (2007), Zeleke et al. (2017), Khanmohammadi et al. (2022), Laz et al. (2023a), Hamdi et al. (2016), Modarres and Ouarda (2014), etc. In meteorological investigation, harmonic analysis is a commonly employed technique for comprehending the dynamics

and evaluating periodic patterns (Raczyński & Dyer, 2023; Rouault et al., 2013). This technique is frequently applied to assess the influence of teleconnections, such as ENSO and QBO, on seasonal variations in meteorological variables, including global precipitation (Chandran et al., 2016; Lee & Julien, 2017; Tarawneh & Kadıoğlu, 2003; Tase, 1976). The harmonic analysis captures temporal fluctuations in time series by modeling sinusoidal patterns at various frequencies, accounting for the diverse frequencies and wavelengths within the data (Asakereh & Razmi, 2012a). Researchers have used this technique to investigate cycles related to both large- and small-scale atmospheric circulation patterns (Dorvlo & Ampratwum, 2000; Kirkyla & Hameed, 1989; Niedźwiedź et al., 2009; Rodriguez et al., 1994). It has been applied across various meteorological parameters, including precipitation (Fetene et al., 2018; Horn & Bryson, 1960; Immerzeel et al., 2005), temperature (Liakatas, 1994; Wang et al., 2018), and precipitable water (Asakereh et al., 2015).

Despite the growing body of research on drought assessment using various methods, there remains a critical gap in understanding long-term spatial and temporal drought variations in the Middle East, especially using high-resolution remote sensing data. Most previous studies have focused on short-term or localized assessments, leaving a lack of comprehensive regional analysis that integrates the impacts of large-scale climatic phenomena. In this study, we utilize the Temperature Vegetation Dryness Index (TVDI) and high-resolution MODIS satellite data to provide a more detailed analysis of drought patterns in the Middle East. Unlike many previous studies, this research investigates the effects of large-scale atmospheric oscillations, such as the El Niño-Southern Oscillation (ENSO) and the Quasi-Biennial Oscillation (QBO), on drought patterns. Additionally, the application of spectral analysis in this study enables the exploration of long-term drought cycles and the identification of more complex climate change patterns, which have been largely overlooked in previous research on the Middle East. Therefore, the primary aim of this research is to conduct a comprehensive spatio-temporal assessment of drought across the Middle East using the Temperature Vegetation Dryness Index (TVDI) derived from MODIS data. This study focuses on providing an in-depth regional drought analysis over a long-term period (2003–2022), examining seasonal, monthly, and annual trends.

Furthermore, it seeks to explore the intricate relationship between land surface temperature and vegetation cover to enhance our understanding of drought dynamics in this region. The research also integrates spectral analysis to detect cyclic drought patterns and investigates their associations with global climatic phenomena such as ENSO and QBO. In sum, this study's novelty lies in its approach to combining high-resolution remote sensing data with TVDI and spectral analysis to unravel complex drought patterns across the Middle East over a substantial timeframe. The

findings of this research could provide new insights for policymakers, environmentalists, and researchers in devising strategies to mitigate drought impacts and adapt to the evolving climate conditions in arid and semi-arid regions.

This paper is organized as follows: Section 2 presents the materials and methods, including a detailed description of the study area and a review of TVDI, the Mann-Kendall test, Sen's slope estimator, and harmonic analysis. The results from the extensive assessment of the various approaches are detailed in Section 3. The discussion is presented in Section 4, and Section 5 provides the study's conclusions.

2. Materials and methods

2.1. Study area

The study area focuses on the Middle East, encompassing sixteen countries: the Arabian Peninsula (Oman, United Arab Emirates, Bahrain, Saudi Arabia, Kuwait, Yemen, and Qatar), Syria, Iran, Palestine, Iraq, Turkey, and Lebanon (Fig. 1a). Situated at the intersection of western Asia and northeastern Africa, the Middle East spans an extensive area of approximately 6,928,000 km² and is home to an estimated population of 320 million. According to land use data and classifications from the International Institute for Applied Systems Analysis (IIASA) and the Food and Agriculture Organization (FAO), the Middle East is largely dominated by bare ground and extensive rangelands, which are indicative of the region's arid and semi-arid landscapes (Fig. 1b). Nevertheless, there are notable exceptions where land cover is more diverse. Specifically, regions such as northeastern Iraq, western Syria, northwestern Iran, Turkey, Lebanon, and the Nile River basin in Egypt display a variety of land uses, including trees, crops, and rangelands (Hameed et al., 2020). These areas benefit from relatively higher precipitation and favorable climatic conditions that foster vegetation growth and sustain agricultural practices. Forested regions, particularly in northern Turkey and Iran, contribute significantly to the land cover diversity in the Middle East (Fallahchai, 2011). Dense vegetation in these areas serves as a vital reservoir of biodiversity and plays an essential role in retaining soil moisture (Croitoru & Liagre, 2013).

Furthermore, regions with substantial water bodies, such as the Tigris and Euphrates river systems, are crucial in supporting adjacent croplands and natural vegetation. In stark contrast, much of the Arabian Peninsula, along with southern Iraq and areas outside the Nile basin in Egypt, is dominated by bare ground and built-up areas. These landscapes are characterized by minimal vegetation cover, resulting from extreme aridity and high temperatures that inhibit plant growth.

The Middle East's climatic conditions range from semi-arid to extremely arid, with vast desert landscapes. Despite this, some areas receive substantial rainfall, particularly in the eastern Mediterranean region and along several mountainous slopes, where annual precipitation can exceed 60 cm (Shoshany & Mozhaeva, 2023). Certain localized areas, such as the southern coast of the Caspian Sea, experience even higher precipitation, reaching up to 180 cm annually (Ghozat et al., 2022). Most of this region's precipitation occurs during the cold season, spanning from November to April, primarily driven by synoptic storm systems. Given the critical role of cold-season precipitation in the region, this study focuses primarily on drought variability associated with these weather phenomena.

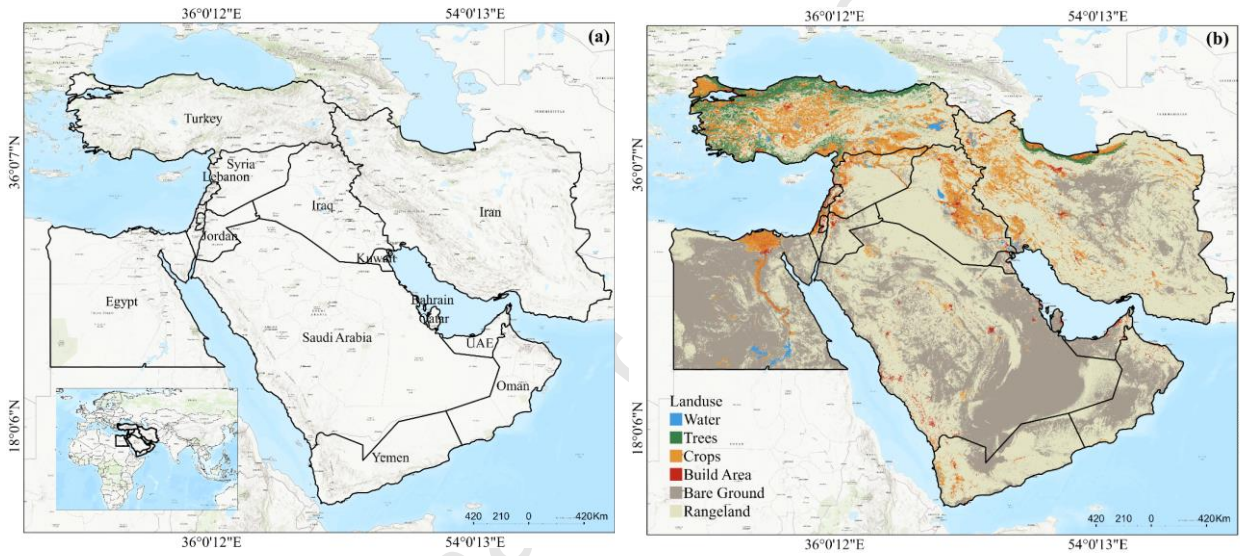

Fig. 1. Study Area Location (a) and Land Use Classification (b) in the Middle East

2.2. Datasets

To accurately monitor and assess drought conditions in the Middle East, this study utilizes satellite-based datasets widely recognized for their reliability in remote sensing applications. This study utilized two data products: LST from MODIS-Aqua and NDVI from MODIS-Terra, both at a spatial resolution of 0.05° (approximately 5.6 km^2) and acquired from 2003 to 2022. These MODIS data products have a well-established track record in assessing drought dynamics (Savtchenko et al., 2004). The Giovanni software (version 4.38) facilitated the data retrieval, an integral component of the NASA Earth Data system, known for its user-friendly interface for accessing geophysical parameters for visualization and analysis (Ganguly, 2016). Additionally, the NDVI data from MODIS is frequently the preferred data source for evaluating vegetation status (Wei et al., 2020). Table 1 provides a detailed overview of the remote sensing data employed in this research

Table 1 Satellite remote sensing products used in this research

Production/title	Time	Unit	Spatial Resolution	Temporal Resolution	Source
LST (MOD11C3)	2003~2022	K	0.05˚(5.6 km)	Monthly	MODIS-Aqua
NDVI (MOD13C2)	2003~2022	-	0.05˚(5.6 km)	Monthly	MODIS-Terra
GPM (IMERGV07)	2003~2022	mm	0.1˚(10 km)	Monthly	NASA GPM
Soil Moisture	2003~2022	m^3 m-3	0.1˚(10 km)	Monthly	FLDAS_NOAH01
EVI (MOD13A2)	2003~2022	-	0.1˚(10 km)	Monthly	MODIS-Terra

2.3. Methodology

A series of remote sensing techniques and statistical analyses were employed to analyze drought conditions in the Middle East. Figure 2 provides a flowchart summarizing the methodology. Subsequent sections will provide a detailed discussion of each step. The application of the Temperature Vegetation Dryness Index (TVDI), which is central to this study, relies on the assumption of homogeneity in climate and land cover conditions across the study area based on the LST-NDVI triangle model. Given the environmental diversity in the Middle East, this study incorporates monthly and seasonal data at various spatial levels (e.g., pixel level). It applies precise statistical techniques, including the Mann-Kendall test and harmonic analysis, to account for regional heterogeneity and ensure the accuracy of TVDI in detecting drought patterns. Additionally, studies conducted in other heterogeneous regions have demonstrated that TVDI performs effectively under such conditions (e.g.,(Du et al., 2017; Tagesson et al., 2018))

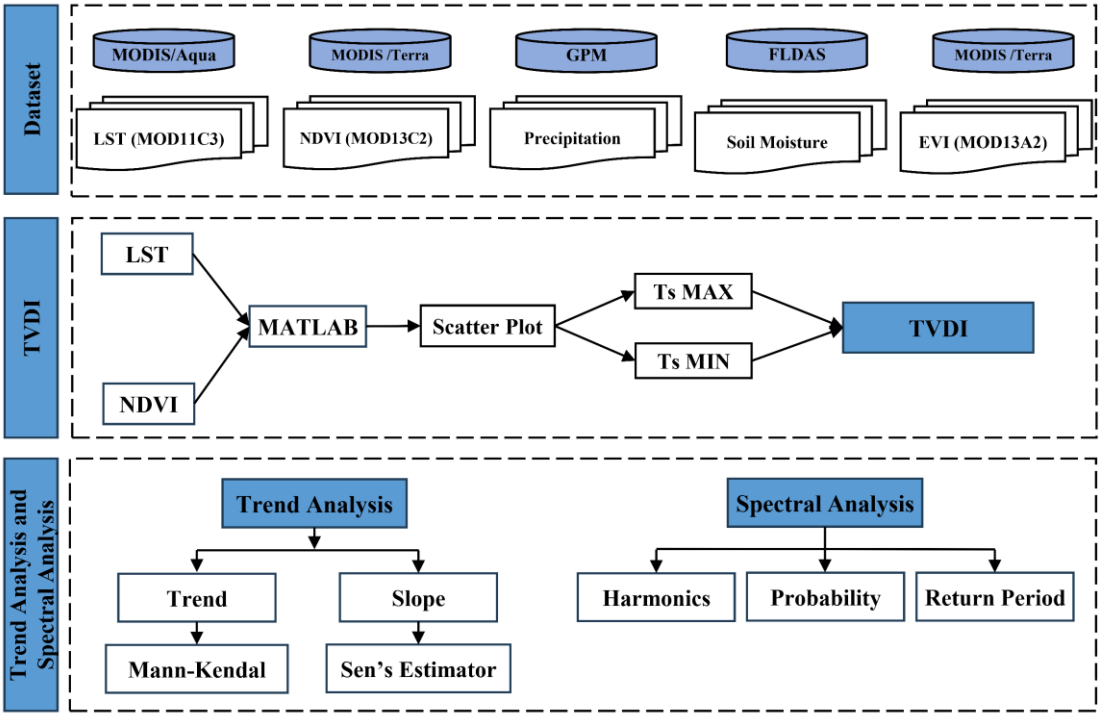

Fig. 2. Flowchart of the proposed methodology

2.3.1. Temperature vegetation dryness index (TVDI)

TVDI utilizes the spatial correlation between Land Surface Temperature (LST) and NDVI to provide insights into drought conditions. The rationale behind using TVDI lies in its ability to represent surface water content through LST variations influenced by vegetation coverage. In areas with bare soil or sparse vegetation, LST responds more acutely to changes in soil moisture, whereas in densely vegetated regions, this response is more gradual, as indicated by higher NDVI values. The TVDI calculation relies on scatterplots illustrating the relationship between LST and NDVI values across pixels, forming a triangular pattern (Sandholt et al., 2002) or a trapezoid (Moran et al., 1994). Figure 3 depicts the typical LST-NDVI triangle, which helps categorize drought conditions across different regions. As illustrated in Fig. 3, the base edge of the triangle, aligned parallel to the NDVI axis, signifies pixels associated with maximum evapotranspiration.

Conversely, the top edge (hypotenuse) indicates pixels exhibiting zero evapotranspiration**,** representing LSTmax within the research area. The space between the triangle's upper and lower edges encompasses diverse evapotranspiration levels linked to varying degrees of drought conditions (Dhorde & Patel, 2016). As the NDVI value increases along the X-axis, the maximum LST proportionally decreases, and this relationship can be characterized by a negative slope using the least squares method, which is performed for each pixel to estimate the coefficients that define the dry edge. In contrast, the wet edge encompasses multiple data points forming horizontal or inclined lines,

indicating various degrees of surface vegetation coverage. Vertically, within the triangular domain where NDVI remains constant, LST gradually increases due to water stress in the surface soil. As observed in previous studies, this transition spans from the minimum LST value (LSTmin) at the wet edge to the maximum (LSTmax) at the dry edge (Du et al., 2017). Simultaneously, the content of surface soil water experiences a corresponding decrease from its maximum to minimum values, as indicated in (Sun et al., 2012). This increases the TVDI from zero to one, marking the shift from extreme wetness to extreme drought in the land surface condition. The formula presented below is employed for the calculation of TVDI (Sandholt et al., 2002):

$$TVDI = \frac{LST - LST_{min}}{LST_{max} - LST_{min}} \quad (1)$$

Where LST is the land surface temperature of each pixel, LST_{min} is the lower horizontal line of the triangle/trapezoid, defining the wet edge; LST_{max} is the maximum surface temperature, defining the dry edge:

$$LST_{min} = a+b\times NDVI \quad (2)$$

$$LST_{max} = c+d\times NDVI \quad (3)$$

Equations 2 and 3 help identify each pixel's wettest and driest conditions, which is crucial for understanding soil moisture variations and drought intensity. These equations, established through pixel-wise linear regression analysis, represent the wet and dry edges. The regression analysis is conducted for each pixel independently to account for local variations in the relationship between NDVI and LST, ensuring precise estimation of LSTmin and LSTmax at the pixel level. The coefficients a, b, c, and d within these equations are derived from the least squares regression fitting method, which is applied to the scatterplot of LST and NDVI for each pixel**.** The scatterplots are divided into specific NDVI intervals, calculated in increments of 0.01, to accurately deduce each interval's maximum and minimum LST values. Such an approach ensures the accurate estimation of drought conditions at the pixel level. The five intensity categories for TVDI are outlined in Table 2.

Table 2 The intensity of drought based on TVDI (Sandholt et al., 2002)

Drought category	Values
Non-drought	TVDI ≤ 0.2
Mild drought	0.21 < TVDI < 0.4
Moderate drought	0.41 < TVDI < 0.6
Severe drought	0.61 < TVDI < 0.8
Extreme drought	0.81 ≤ TVDI < 1

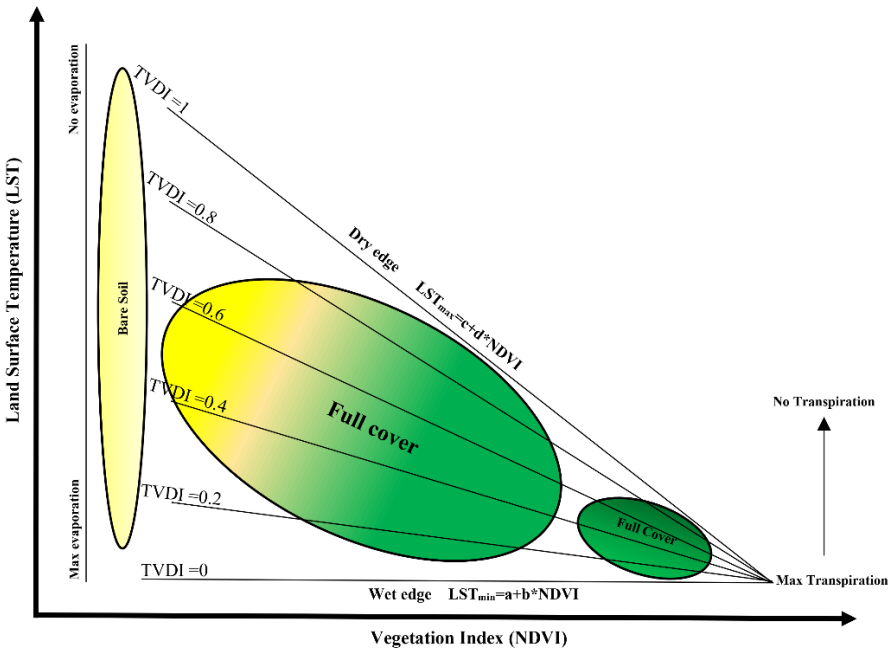

Fig. 3. Simplified LST and NDVI triangle.

2.3.2. Enhanced Vegetation Index (EVI)

EVI was developed to offer an improved monitoring of vegetation health and dynamics. Unlike NDVI, which is sometimes interfered with by atmospheric conditions or even interference from the Earth's surface beneath the vegetation cover, EVI includes adjustments that reduce these effects (Schnur et al., 2010). This makes EVI a strong tool for monitoring vegetation health in various environments, even in areas comprising densely richly vegetated regions (Huete et al., 2002).

This study employed the MOD13A2 product from MODIS, which provides EVI values every 16 days at a resolution of 1 km. This data product represents stable, global-scale measurements and is appropriate for monitoring vegetation patterns over large areas such as the Middle East. Specifically, the high temporal and spatial resolution is suitable for studying green vegetation's response to climatic variation, particularly in semi-arid and arid regions (Chen et al., 2024).

The EVI calculation used in this study is described by the following formula (Mokarram & Zarei, 2023):

$$EVI = G \times \frac{(NIR - RED)}{(NIR + C1 \times RED - C2 \times BLUE + L)} \quad (4)$$

In this formula, NIR, RED, and BLUE represent the reflectance values in each of these wavebands; G is a gain factor that scales the index; L is a term that corrects for reflectance from the soil background; and C_1 and C_2 are coefficients that correct for atmospheric interference.

2.3.3. Mann-Kendall Test

The Mann-Kendall (MK) test was employed to detect trends in time series data. This non-parametric statistical test, originally introduced separately by Mann (1945) and Kendall (1975), is widely recognized as a standard method for analyzing trends in time series data (Demirgül et al., 2022; Fiala et al., 2010; Gebremicael et al., 2017; Ghaderpour et al., 2024; Ouarda et al., 2021; Páscoa et al., 2020; Shawky et al., 2023). This test offers several advantages: 1) The analysis does not require data to follow a specific distribution, making it amenable to datasets containing extreme values (Hirsch et al., 1992), 2) Missing values are permissible within the analysis (Yu et al., 1993), 3) The test relies on the relative magnitudes (ranking) of data points rather than their numerical values. This feature accommodates "trace" or "below detection limit" data by assigning them values less than the smallest measured value (Zhai & Feng, 2009), and 4) MK analysis for time series does not necessitate the assumption of linearity in the trend, making it a versatile tool for trend assessment (da Silva, 2004; Sneyers, 1990). The MK test is given as:

$$S = \sum_{i=1}^{n-1} \sum_{j=i+1}^{n} \operatorname{sgn}(x_j - x_i) \quad (4)$$

The trend test is applied to a time series, denoted as x_i, where i ranges from 1 to n-1. For each data point, x_i is taken as a reference point and compared with the remaining data points, x_j, where j ranges from i+1,2,...,n. This process is performed as follows:

$$\operatorname{sgn}(x) = \begin{cases} +1 & \text{if } (x_j - x_k) > 0 \\ 0 & \text{if } (x_j - x_k) = 0 \\ -1 & \text{if } (x_j - x_k) < 0 \end{cases} \quad (5)$$

It has been established that when *n* is greater than or equal to 8, the statistic *S* approximately follows a normal distribution with a mean. The variance of this statistic is given by:

$$\operatorname{Var}(s) = \frac{n(n-1)(2n+5) - \sum_{i=1}^{n} t(t-1)(2t+5)}{18} \quad (6)$$

Where t_i represents the number of tied values up to sample *i*. The test statistic Z_c is calculated as:

$$Z_{MK} = \begin{cases} \dfrac{S-1}{\sqrt{Var(s)}} & if \quad S > 0 \\ 0 & if \quad S = 0 \\ \dfrac{S+1}{\sqrt{Var(s)}} & if \quad S < 0 \end{cases} \quad (7)$$

Positive values of Z_{MK} indicate increasing trends, whereas negative Z_{MK} values indicate decreasing trends in the time series. When $|Z_{MK}| > Z_{1-\alpha/2}$, the null hypothesis is rejected, signifying the presence of a significant trend in the time

series. For a 5% significance level, the critical value $Z_{1-\alpha/2}$ is 1.96. In this study, the MK test was computed using the MATLAB software.

2.3.4. Sen's slope estimator

Sen's slope estimator is used to quantify the magnitude of the trend. This involves calculating the slope (T_i) for each pair of data points, and it follows the methodology introduced by Sen (1968).

$$T_i = \frac{X_j - X_k}{j - k} \qquad for\ i = 1,2, \ldots\ldots, N \quad (8)$$

In this context, X_j and X_k refer to the data values at times j and k, with j being greater than k. The median of the N values of T_i is defined as Sen's estimator of the slope, and it is expressed as:

$$Q_i \begin{cases} T_{\frac{N+1}{2}} & N\ is\ odd \\ \frac{1}{2}\left(T_{\frac{N}{2}} + T_{\frac{N+2}{2}}\right) & N\ is\ even \end{cases} \quad (9)$$

Sen's estimator is calculated as $Q_{med} = \frac{T(N1)}{2}$ when N is an odd value. In the case of an even N, it is computed as $Q_{med} = \left[T_{\frac{n}{2}} + T_{\frac{n+2}{2}}\right]/2$. Subsequently, Q_{med} is determined using a two-sided test at a 100 (1- α) % confidence level, allowing us to establish the true slope through a non-parametric test. A positive Q_i value signifies an upward or increasing trend, while a negative Q_i value indicates a downward or decreasing trend within the time series. According to Ahani et al. (2012), if a time series presents a linear trend, the true slope (change per unit time) can be estimated by using a simple non-parametric procedure developed by Sen (1968). All Sen's slope estimator calculations have been done using MATLAB software.

2.3.5. Spectral Analysis

Spectral analysis is a powerful tool for identifying the periodic components within a time series, offering valuable insights into the cyclical patterns of drought occurrences. This technique first transforms the time series data into a frequency domain, represented as periodic functions characterized by their amplitudes and frequencies. This method provides a deeper understanding of the dominant cycles influencing drought variability in the Middle East. The initial step in spectral analysis is decomposing the time series into its constituent waveforms. In this context, "frequency" corresponds to the number of cycles occurring per unit of time, while "amplitude" indicates the magnitude of variation

at each frequency. In the process of spectral analysis, all constituent waves are initially isolated. Following this, the individual contributions of each wave to the total variance are determined, and subsequently, the statistical significance of each wave is evaluated (Ghaemi et al., 2017). To compute the harmonics effectively, it is imperative to assess the following two crucial parameters (Chatfield, 2013):

$$a_i = \frac{2}{n}\sum_{t=1}^{n} X_t \cos\left(\frac{2\pi q}{n}t\right) \quad q=1,2,\ldots,\frac{n}{2} \quad (10)$$

$$b_i = \frac{2}{n}\sum_{t=1}^{n} X_t \sin\left(\frac{2\pi q}{n}t\right) \quad t=1,2,\ldots,n \quad (11)$$

In the context of our study, the variable "q" signifies the count of harmonics being examined. The quantity of harmonics differs based on whether the time series is even or odd. In the case of an even time series, the number of harmonics, denoted as "q," can be expressed as q = (n-1) / 2, whereas for an odd time series, q = n / 2 harmonics. Subsequently, the dispersion of variance for each of these harmonics is computed through the following mathematical formulation:

$$I(f_i) = \frac{n}{2}\ (a_i^2 + b_i^2) \qquad i = 1,2,\ldots\ldots,q \quad (12)$$

The significance test of the spectral is performed using the chi-square (χ^2) test with degrees of freedom, as expressed in the following relationship:

$$df = \frac{2n - \frac{q}{2}}{q} \quad (13)$$

A critical aspect of the spectral analysis technique entails the examination of the null hypothesis. For the spectral analysis, the null hypothesis posits the absence of a significant deviation from zero at a particular frequency. To address this, it is recommended to compute the first-order autocorrelation for the time series data, denoted as "r_1" (Torres & Warde, 2017). Should the first-order autocorrelation fail to exhibit a statistically significant departure from zero, it becomes necessary to consider a time series devoid of any discernible trend. In such instances, the null hypothesis of white noise is deemed appropriate (Asakereh et al., 2014). However, given that the first-order autocorrelation, "r_1," in climatic time series data often demonstrates a significant deviation from zero, indicating a null hypothesis of red noise, the evaluation of "r_1" is imperative based on the correlation coefficient and harmonics (i $\leq 0 \leq$ q) employing the subsequent approximation, as outlined by Mitchell Jr (1966):

$$\lambda_k = \bar{S}\left[\frac{1 - r^2}{1 + r_1^2 - 2r_i \cos\frac{\pi k}{q}}\right] \quad (14)$$

Within the presented equation, the variable "S" denotes the mean of all unprocessed spectral estimates, considering the statistical significance of "r_1." To assess the significance of the spectral, an initial step involves considering a confidence interval, typically set at 95%. Subsequently, the evaluation of the spectral's significance is performed utilizing the subsequent formula (Schickedanz & Bowen, 1977):

$$\lambda_k \frac{X_v^2(0.95)}{v} \leq \hat{I}(f) \leq \lambda_k \frac{X_v^2(0.05)}{v} \quad (15)$$

Therefore, any frequencies within the spectra of the time series that extend beyond the confines of the confidence interval may be considered statistically significant at the predetermined confidence level and the corresponding frequency. A commonly utilized technique for visualizing spectral fluctuations, the frequencies of cyclical occurrences, and the significance of time series in the spectral analysis methodology is the application of a periodogram.

3. Results

3.1 Trend analysis of TVDI

The Mann-Kendall test and Sen's slope estimator were applied to assess TVDI trends using monthly, seasonal, and annual data for 258,087 pixels in the Middle East. Interpolated maps were generated using the kriging method in ArcGIS 10.6, with selection based on error assessment criteria, including cross-validation, root mean square error (RMSE), and R^2. As outlined in Figs. 4 to 9, the trend and slope maps for TVDI at various temporal scales identify areas exhibiting increasing, decreasing, or no significant trends at a 95% confidence level, along with the magnitude of the TVDI slope changes. The monthly trend maps (Fig. 4) offer a comprehensive view of the spatial distribution of TVDI trends across the Middle East. In January, upward trends are primarily concentrated in the north, covering areas like Turkey, western Iran, and Syria, while the southern regions, notably Egypt and Saudi Arabia, display stable or downward trends. February reveals an intensification of upward trends in northern areas, extending into northern Iraq and parts of Jordan. At the same time, southwestern regions, particularly Egypt and Yemen, show increased downward trends.

The most pronounced upward trends appear in March, concentrated in Turkey, Iraq, and western Iran, contrasting with the generally stable or slightly downward trends in central and southern parts. April maintains strong upward trends in northern areas, notably Turkey, Syria, and Iraq, with the south continuing to exhibit stable or downward trends. A shift begins in May, as extensive downward trends emerge across southern and central parts of the Middle East, affecting areas like Saudi Arabia, Egypt, and Oman, while upward trends remain persistent in the northern areas,

especially Turkey and northwestern Iran. By June, a significant shift sees downward trends dominating most of the Middle East, leaving only isolated northern areas with slight upward trends. The strongest downward trends across the region occur in July, particularly in Saudi Arabia, Oman, and parts of the UAE, although minor upward trends linger in Turkey and northern Iran. In August, the dominance of downward trends continues, with slight upward trends in northern Turkey and parts of Iran, suggesting a relative stabilization in soil moisture. Downward trends prevail in September, showing minimal upward trend intensity, particularly in regions like Saudi Arabia, Egypt, and the UAE. Upward trends reappearance occurs in northern regions in October, especially Turkey and Iraq, while minimal downward trends are noted in the southern and central areas. November sees a renewed concentration of upward trends in Turkey and northwestern Iran, whereas the southern areas, including Oman and Yemen, mostly experience stable or slightly downward trends. Finally, in December, upward trends continue in northern areas like Turkey and parts of Iran, while southern regions, particularly Egypt, Saudi Arabia, and Yemen, maintain a pattern of stable or downward trends.

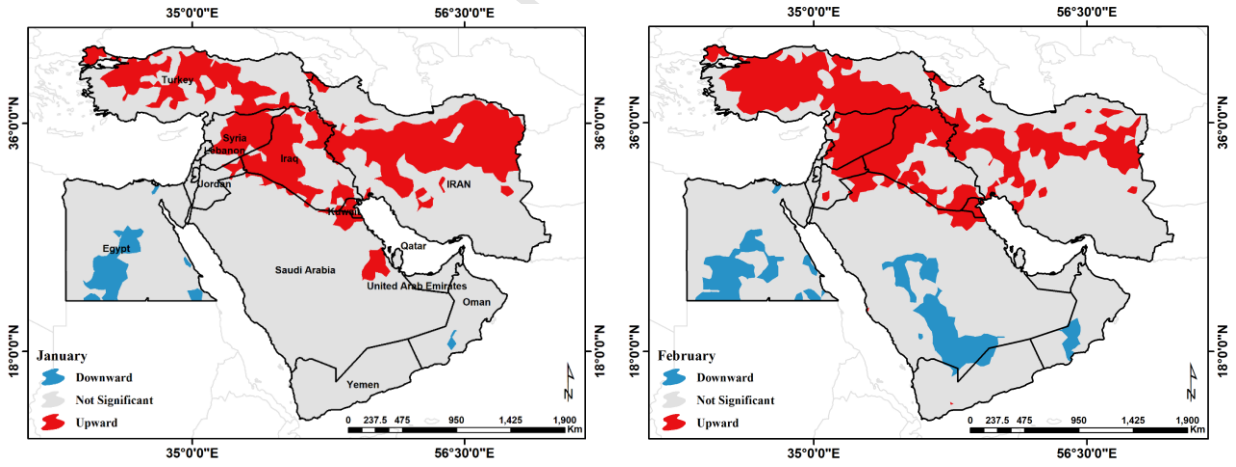

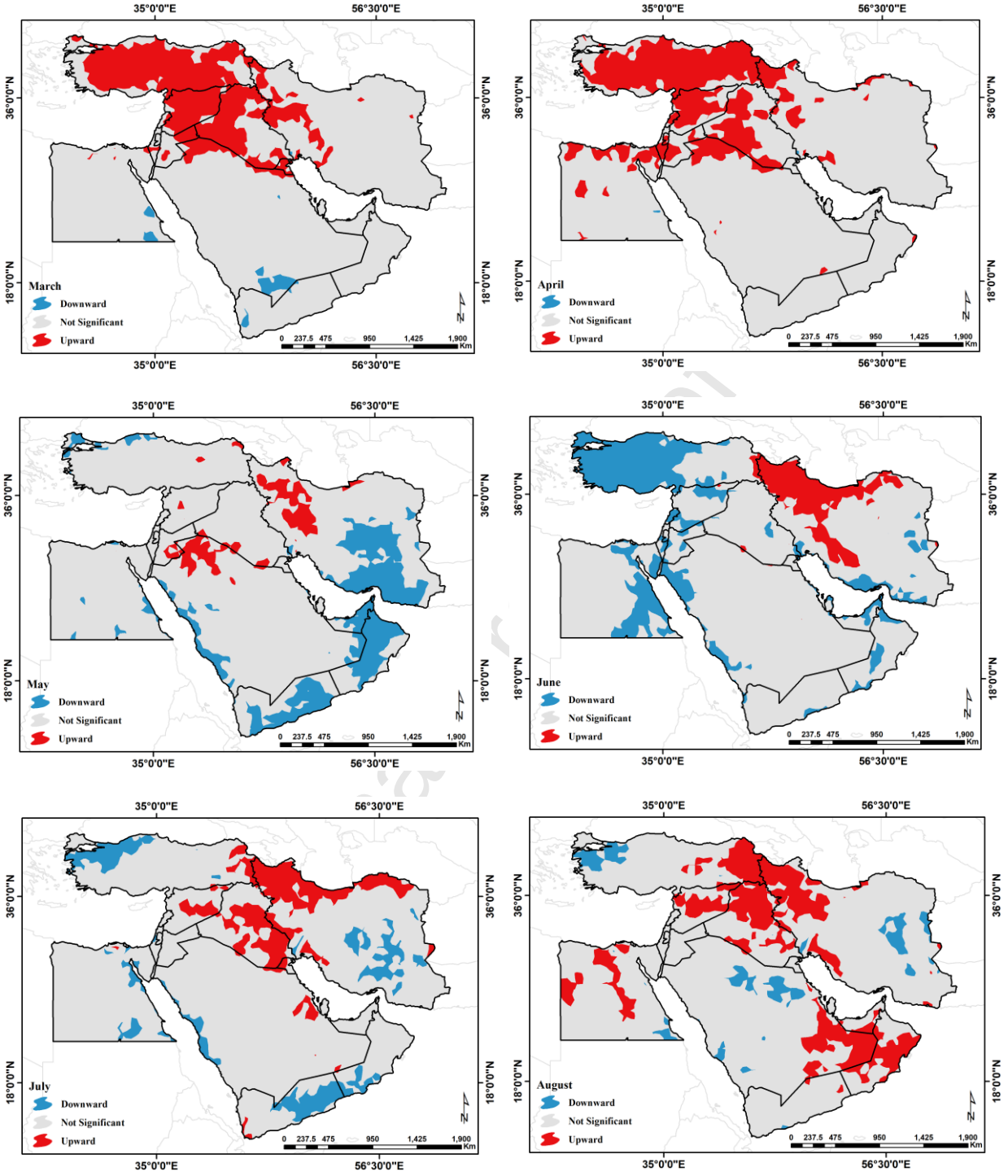
35°0'0"E
56°30'0"E
36°0'0"N
18°0'0"N
March
Downward
Not Significant
Upward
0 237.5 475 950 1,425 1,900
Km
April
May
June
July
August

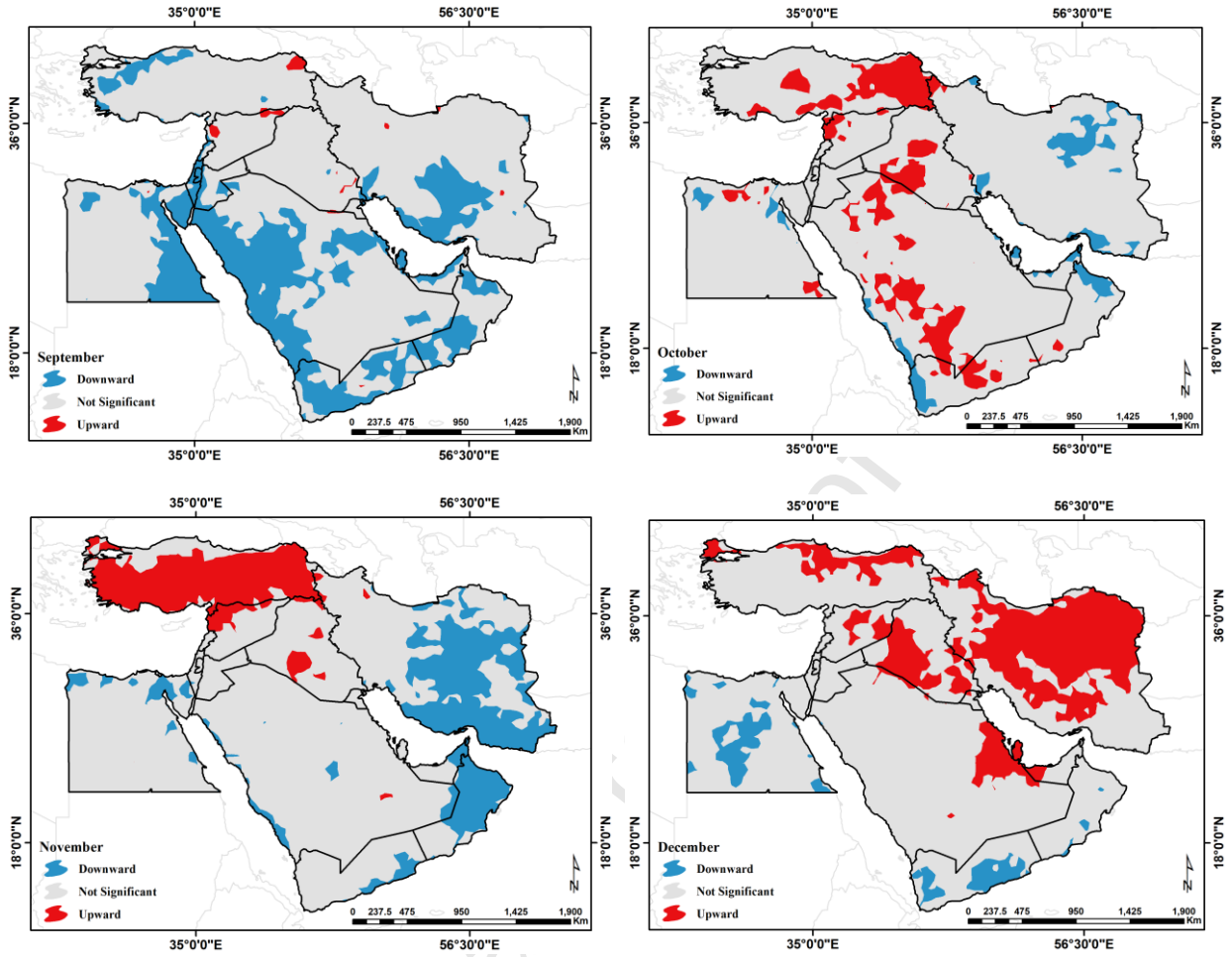

Fig. 4. Spatial distribution of monthly TVDI trend in the Middle East

The seasonal analysis of TVDI trend maps reveals distinctive patterns across the Middle East (Fig. 5). During the winter season, most parts of the region show no significant TVDI trends, indicating stable moisture conditions. Some isolated areas in the northern regions, such as Turkey and northwestern Iran, show slight upward trends, reflecting a mild increase in dryness levels. As the region transitions from winter to spring, the southern, western, and northwestern areas display significant downward trends in TVDI, suggesting improved soil moisture. In contrast, certain central areas, particularly northwestern Iran and western Iraq exhibit upward trends, indicating increased dryness in these regions. In the summer, a dominant pattern of significant downward trends appears across much of the Middle East, indicating improved soil moisture conditions despite the extreme heat. This pattern is observed in areas like Saudi Arabia, Iraq, and southeastern Iran. During the autumn, the extent of areas with downward trends diminishes, while upward trends become more concentrated, especially in Turkey and western Iran, where dryness intensifies as rainfall decreases.

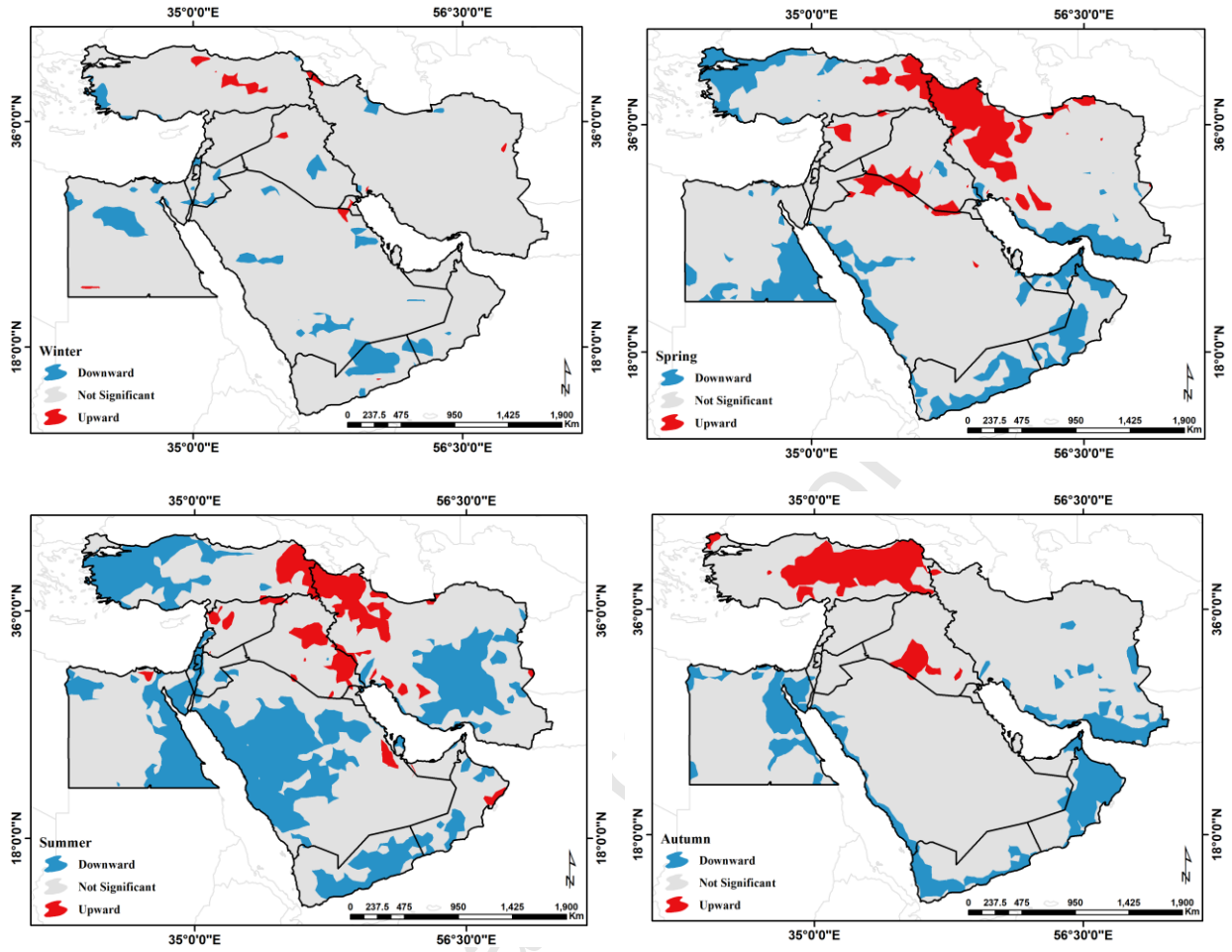

Fig. 5. Spatial distribution of seasonal TVDI trend in the Middle East

The annual TVDI trend map (Fig. 6) highlights that, over the study period, most regions in the Middle East, particularly those between latitudes 13° and 26°, have experienced a declining trend in TVDI. This downward trend is evident in the monthly trend change maps as well. In contrast, only the northern parts of the Middle East, including northwestern Iran and western Turkey, exhibit an upward trend in TVDI. The annual trend map thus indicates a long-term declining trend in TVDI for most regions below latitude 34°.

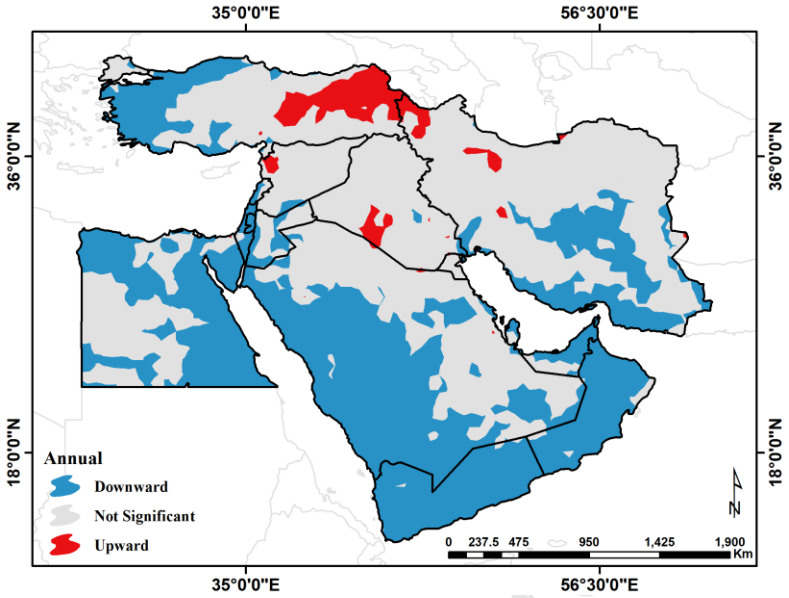

Fig. 6. Spatial distribution of annual TVDI trend in the Middle East

The monthly Sen's slope maps (Figs. 7 to 9) demonstrate notable variations in the slope values of TVDI trends across different seasons, with significant upward and downward trends observed depending on the month and geographic location. January displays moderate upward slopes across northern areas, particularly in Turkey, Syria, and parts of Iraq, while most Saudi Arabia, Oman, and southern regions exhibit modest downward slopes. February shows a slight intensification in the upward slopes in the north, with Turkey and northwestern Iran experiencing increased dryness. Meanwhile, Egypt and Yemen display downward slopes, suggesting some moisture retention. In March, upward slope trends become more pronounced, especially across northwestern Iraq and parts of Syria, reflecting the gradual onset of drier conditions as the region transitions into spring. Central areas, including southern Saudi Arabia and Yemen, continue to display downward slopes, indicating persistent moisture levels in these regions. April shows the highest upward slopes overall, reaching up to 0.22 in areas of Turkey and northern Iraq, marking the peak of aridity in these regions as temperatures rise. During May, slope values indicate a shift, with downward slopes dominating southern regions, such as Egypt and the Arabian Peninsula, while upward trends persist in northern territories like Turkey and northwestern Iran, where dryness remains prevalent. June features predominantly downward trends across the Middle East, though notable upward slopes remain in isolated northern areas, including northern Iraq and Syria. July presents the steepest downward slopes across the Middle East, particularly in southern regions such as Saudi Arabia, Oman, and the UAE, where increased heat and aridity dominate. August reveals a slight moderation in the downward slopes across southern regions, while upward trends remain minimal but continue in northern areas, indicating a relative stabilization in dryness. In September, the downward slopes were widespread across the Middle East, particularly in

central Saudi Arabia, the center of Iran, and Egypt, where notable moisture improvement was observed. Upward trends remain largely absent. October shows the reemergence of upward slopes, particularly in Turkey and western Iraq, as cooler temperatures begin to set in, while southern regions display stable or minimal downward slopes, indicating residual moisture from the warmer months. By November, upward slopes intensify significantly in Turkey and northwestern Iran, signifying increased dryness in these regions. Downward slopes, however, continue to dominate the southern half of the Middle East, reflecting retained soil moisture in response to cooling temperatures. Finally, December shows the lowest slopes for both upward and downward trends, with only slight upward slopes in the northern areas and minimal downward trends in the southern parts, suggesting overall moisture stability across the region as winter begins.

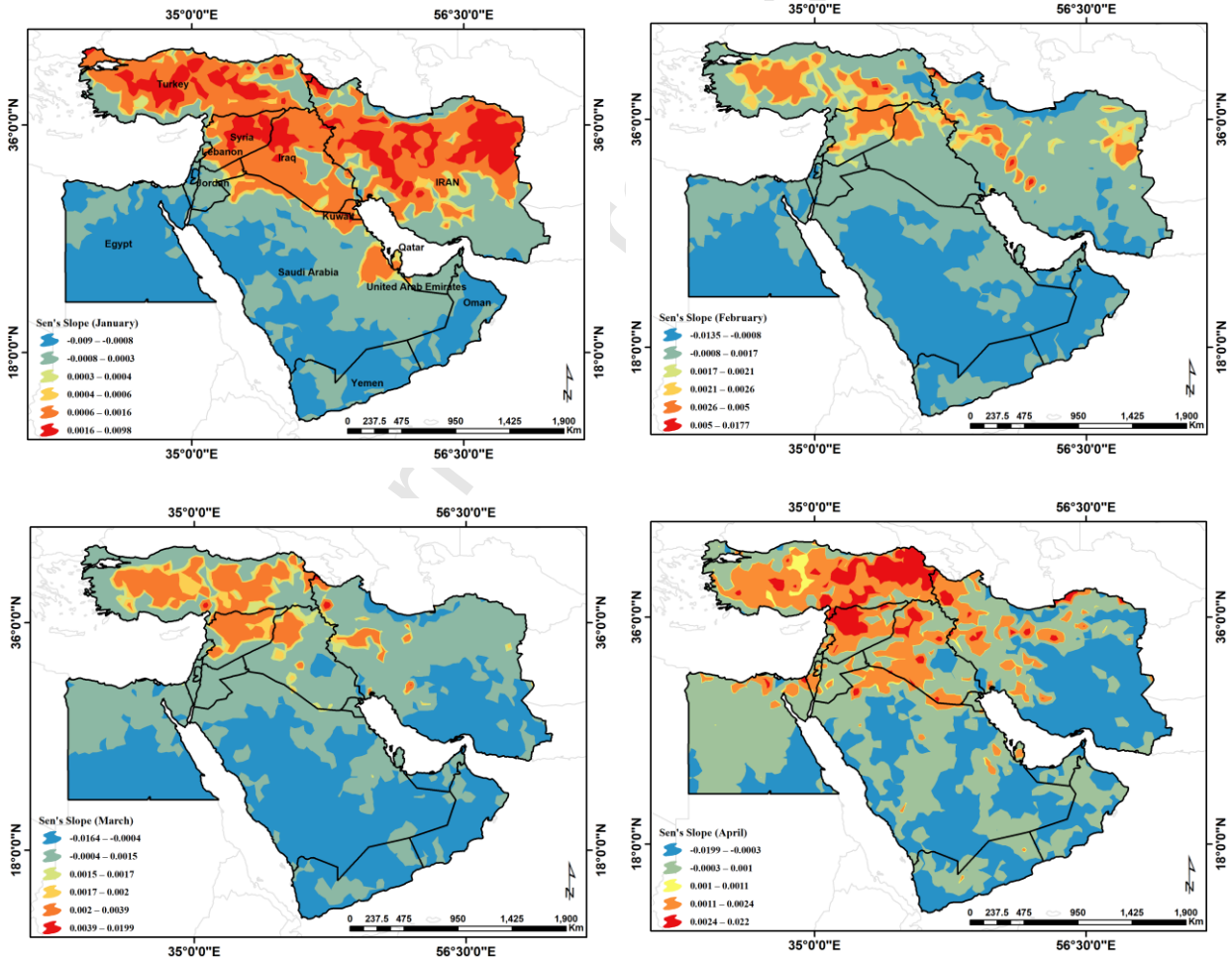

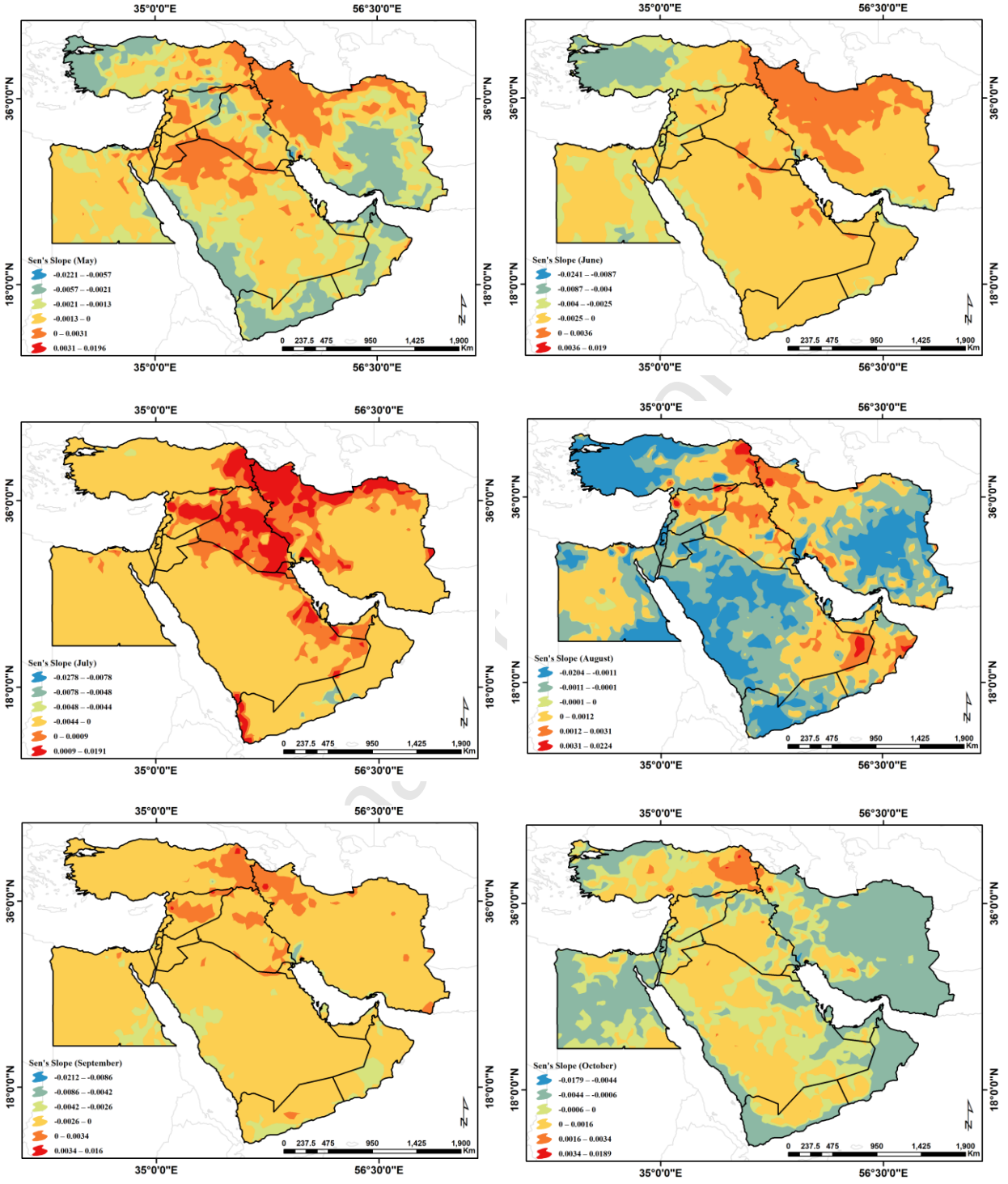
35°0'0"E
56°30'0"E
36°0'0"N
18°0'0"N
Sen's Slope (May)
-0.0221 – -0.0057
-0.0057 – -0.0021
-0.0021 – -0.0013
-0.0013 – 0
0 – 0.0031
0.0031 – 0.0196
Sen's Slope (June)
-0.0241 – -0.0087
-0.0087 – -0.004
-0.004 – -0.0025
-0.0025 – 0
0 – 0.0036
0.0036 – 0.019
Sen's Slope (July)
-0.0278 – -0.0078
-0.0078 – -0.0048
-0.0048 – -0.0044
-0.0044 – 0
0 – 0.0009
0.0009 – 0.0191
Sen's Slope (August)
-0.0204 – -0.0011
-0.0011 – -0.0001
-0.0001 – 0
0 – 0.0012
0.0012 – 0.0031
0.0031 – 0.0224
Sen's Slope (September)
-0.0212 – -0.0086
-0.0086 – -0.0042
-0.0042 – -0.0026
-0.0026 – 0
0 – 0.0034
0.0034 – 0.016
Sen's Slope (October)
-0.0179 – -0.0044
-0.0044 – -0.0006
-0.0006 – 0
0 – 0.0016
0.0016 – 0.0034
0.0034 – 0.0189
0 237.5 475 950 1,425 1,900
Km

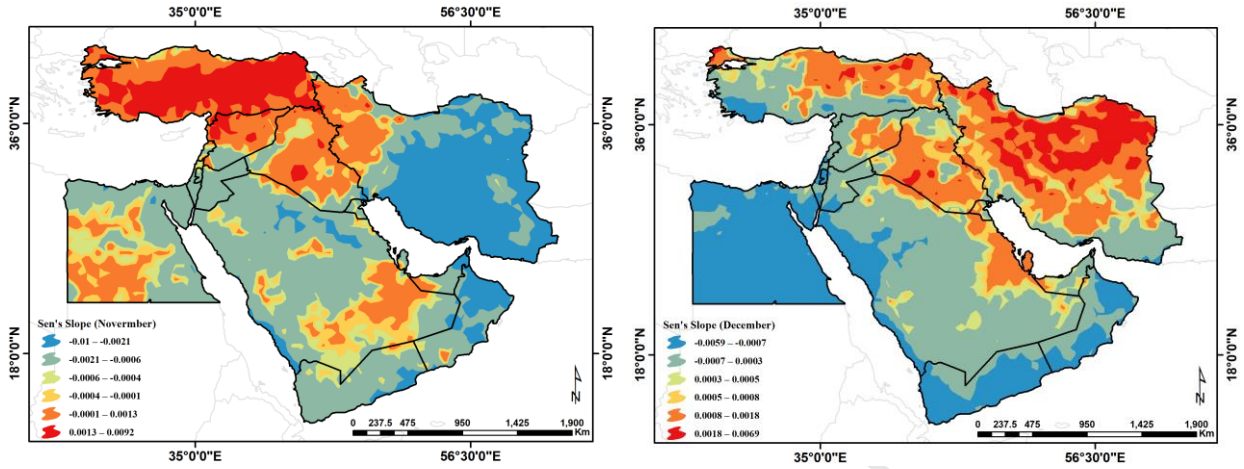

Fig. 7. Spatial distribution of slope changes in the TVDI monthly trend in the Middle East

The seasonal analysis of Sen's slope maps reveals distinct patterns across the Middle East (Fig. 8). In spring, the highest positive slope values are observed, reaching up to 0.0209 in central regions such as western Iran, Iraq, Syria, eastern Turkey, and northern Saudi Arabia, indicating a notable upward trend in TVDI in these areas. The seasonal analysis of Sen's slope maps reveals distinct patterns across the Middle East. In spring, the highest positive slope values are observed, reaching up to 0.0209 in central regions such as western Iran, Iraq, Syria, eastern Turkey, and northern Saudi Arabia, indicating a notable upward trend in TVDI. During summer, significant negative slope values dominate the southern and central parts of the region, particularly in areas like southern Iran, southern Saudi Arabia, and southern Egypt, with values dropping as low as -0.0205. In autumn, positive slope values remain high in certain northern and central areas, including parts of Turkey, Iraq, and western Iran, while moderate negative slopes continue to appear in southern regions. Winter displays the mildest downward trend, with negative slope values as low as -0.0104 across the southern and central regions, including Egypt, the Arabian Peninsula, and southern Iran, reflecting a reduction in negative slope intensity compared to the warmer seasons. This seasonal analysis highlights the spatial and temporal variability in TVDI trends across the Middle East, with pronounced shifts in slope intensity between warmer and cooler seasons.

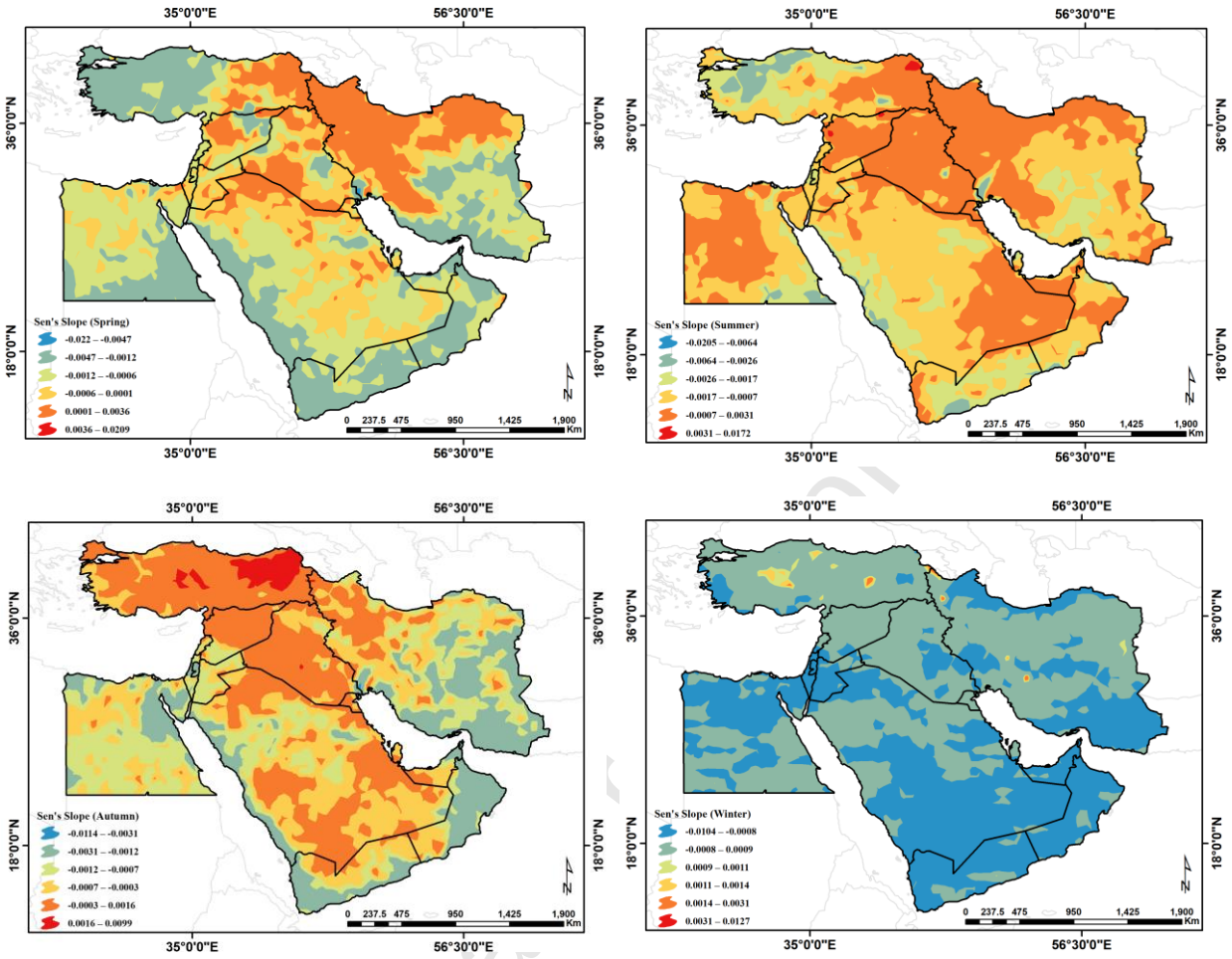

Fig. 8. Spatial distribution of slope changes in the TVDI seasonal trend in the Middle East

The annual slope maps (Fig. 9) divide the study region into two distinct segments. The southern, eastern, and western parts of the Middle East exhibit negative slope variations, while the central and northern regions (except for western Turkey) show positive slope trends.

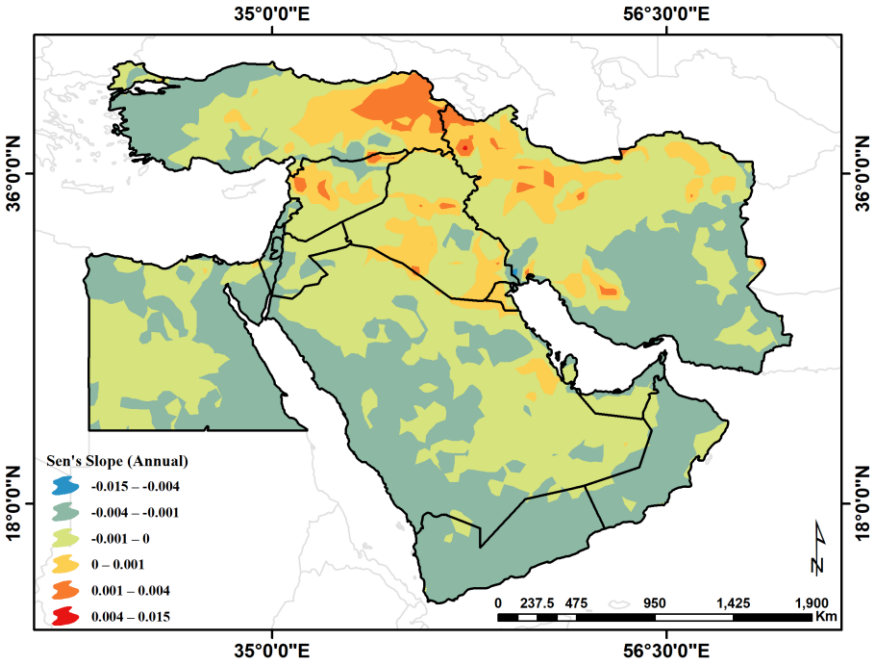

Fig. 9. Spatial distribution of slope changes in the TVDI annually trend in the Middle East.

3.2 Spectral analysis of TVDI

By applying spectral analysis to the TVDI values of 26 selected stations in the Middle East, the significance of each cycle at a 95% confidence level was assessed by plotting TVDI periodograms for each station individually. Fig. 10 presents the spectra and confidence intervals for the TVDI time series at the selected stations. In these figures, the lower horizontal axis represents frequency (or harmonic), the upper horizontal axis shows the return period for each frequency, and the vertical axis represents the variance of each cycle. The solid and dashed lines above indicate the significance boundary for the 95% confidence level. When a cycle crosses the significance boundary, it indicates the non-randomness of that cycle, while failure to cross the boundary suggests that the cycle is random.

The results reveal multiple cycles with varying return periods at most stations (Table 3). Significant cycles indicate the emergence of specific patterns that demonstrate coherent TVDI values in cyclic forms. In particular, when a cycle crosses the significance boundary, it signifies a periodic pattern that holds statistical relevance, confirming that the observed behavior is not due to random variation. However, stations such as Al Basra, Al Riyadh, Baghdad, Istanbul, Mosul, and Shiraz do not show distinct cycles. In these cases, the spectral variances across all harmonics are approximately equally distributed, and at the 95% confidence level, no significant cycles are detected. This lack of significant cycles suggests a random data distribution, indicating that these stations do not exhibit dominant or synchronous TVDI behaviors, and the variance does not correlate with any regular period.

In contrast, periodograms for other stations, such as Adana, Al Kuwayt, Al Madinah, Amman, Cairo, and Tehran, display non-sinusoidal cycles with return periods equal to the length of the statistical period. For instance, stations like Abu Dhabi and Masqat reveal periodic patterns with shorter return periods, specifically around 2.6 years, indicating a frequent cyclic behavior at these locations. Moreover, the periodograms for stations such as Cairo, Amman, and several others, including Adana, Al Kuwayt, Doha, and Tehran, reveal significant cycles with moderate return periods of around 20 years. These cycles might be influenced by broader climatic patterns rather than short-term seasonal variability, suggesting a regional climatic influence across these locations. This contrasts with patterns in places like Esfahan, which also shows a significant 20-year cycle, potentially reflecting longer-term climatic variability related to soil moisture conditions. In contrast, Tabriz displays low variance across all frequencies, indicating less-defined cyclic behaviors and an absence of a strong periodic structure.

Table 3 The statistical characteristics of the annual TVDI cycles in selected stations

Station	Significant harmonic(s)	Probability	Return period	Station	Significant harmonic(s)	Probability	Return period
AbuZaby	7	0.35	2.6	Baghdad	-	-	-
Adana	1	0.06	20	Beirut	9	0.47	2.1
Al Basra	-	-	-	Cairo	1	0.06	20
Al Kuwayt	1	0.06	20	Doha	1	0.06	20
Zahedan	8	0.42	2.3		9	0.47	2.1
Al Madinah	1	0.06	20	Erzurum	5	0.26	3.7
Al Riyadh	-	-	-	Ankara	4	0.23	5
Amman	1	0.06	20	Esfahan	1	0.06	20
Tehran	1	0.06	20		8	0.42	2.3
Jiddah	2	0.12	9	Mosul	-	-	-
Aswan	1	0.06	20	Homes	3	0.17	5.5
	4	0.23	5	Shiraz	-	-	-
Istanbul	-	-	-	Masqat	7	0.35	2.6
Mashhad	1	0.06	20	Tabriz	1	0.06	20
Sanaa	-	-	-		9	0.47	2.1

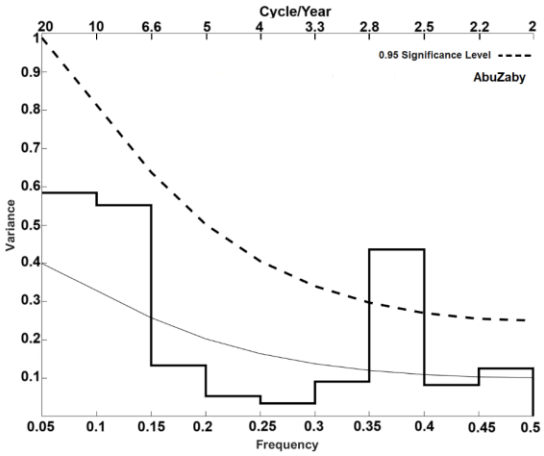
Cycle/Year
20 10 6.6 5 4 3.3 2.8 2.5 2.2 2
0.95 Significance Level
AbuZaby
Variance
Frequency
0.05 0.1 0.15 0.2 0.25 0.3 0.35 0.4 0.45 0.5

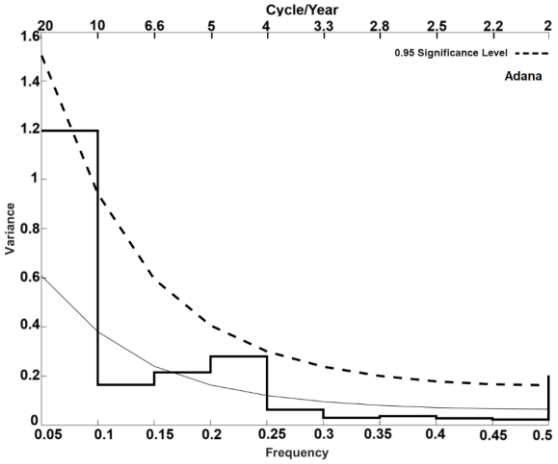
Cycle/Year
20 10 6.6 5 4 3.3 2.8 2.5 2.2 2
0.95 Significance Level
Adana
Variance
Frequency
0.05 0.1 0.15 0.2 0.25 0.3 0.35 0.4 0.45 0.5

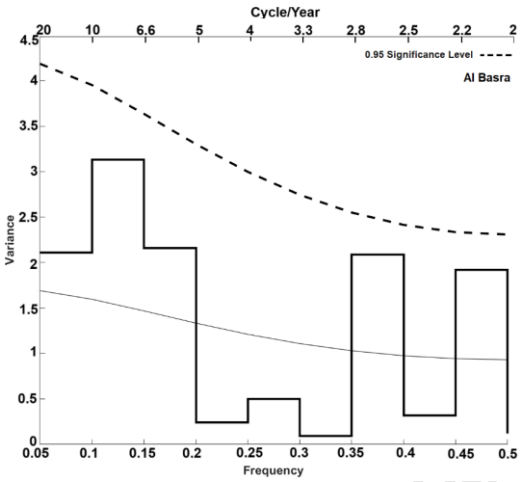
Cycle/Year
20 10 6.6 5 4 3.3 2.8 2.5 2.2 2
0.95 Significance Level
Al Basra
Variance
Frequency
0.05 0.1 0.15 0.2 0.25 0.3 0.35 0.4 0.45 0.5

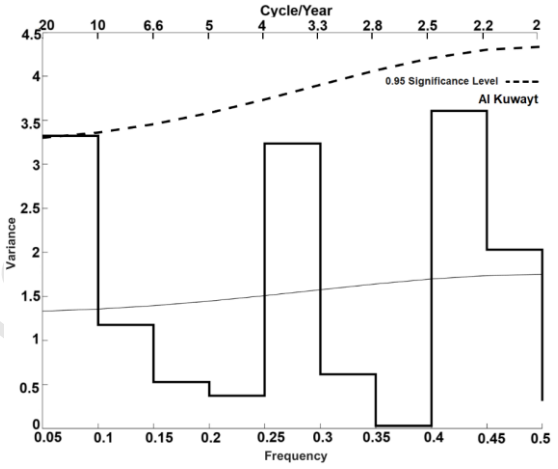
Cycle/Year
20 10 6.6 5 4 3.3 2.8 2.5 2.2 2
0.95 Significance Level
Al Kuwayt
Variance
Frequency
0.05 0.1 0.15 0.2 0.25 0.3 0.35 0.4 0.45 0.5

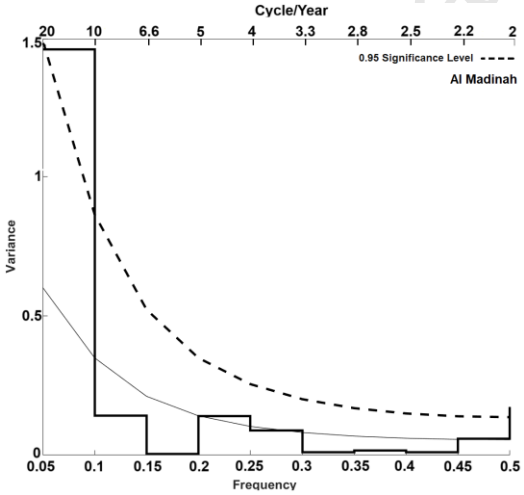
Cycle/Year
20 10 6.6 5 4 3.3 2.8 2.5 2.2 2
0.95 Significance Level
Al Madinah
Variance
Frequency
0.05 0.1 0.15 0.2 0.25 0.3 0.35 0.4 0.45 0.5

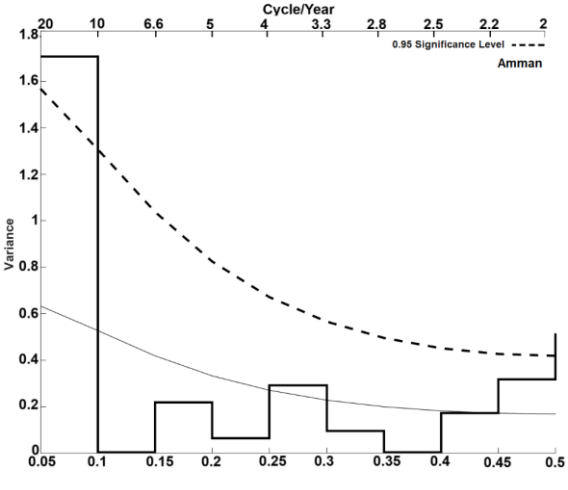
Cycle/Year
20 10 6.6 5 4 3.3 2.8 2.5 2.2 2
0.95 Significance Level
Amman
Variance
0.05 0.1 0.15 0.2 0.25 0.3 0.35 0.4 0.45 0.5

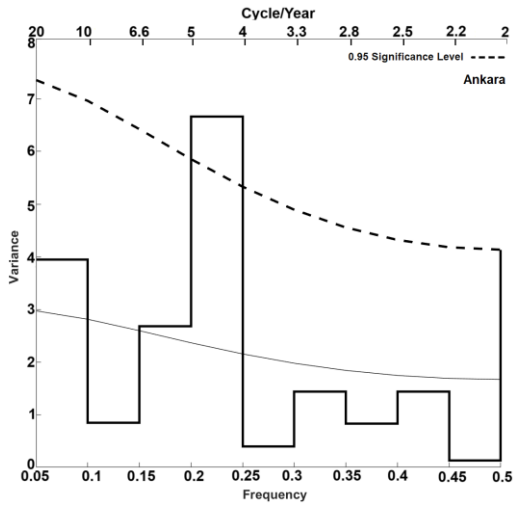
Cycle/Year
20 10 6.6 5 4 3.3 2.8 2.5 2.2 2
0.95 Significance Level
Ankara
Variance
Frequency
0.05 0.1 0.15 0.2 0.25 0.3 0.35 0.4 0.45 0.5

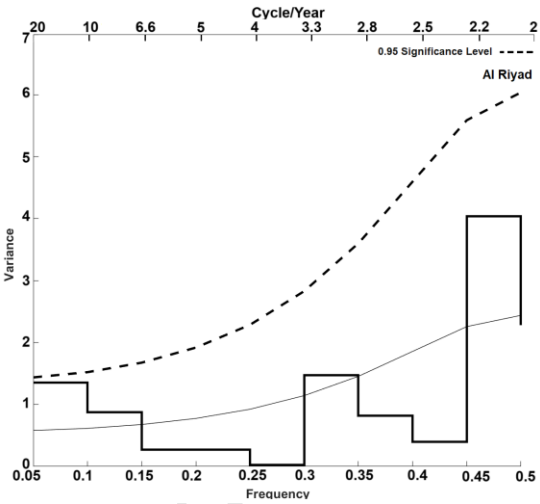
Cycle/Year
20 10 6.6 5 4 3.3 2.8 2.5 2.2 2
0.95 Significance Level
Al Riyad
Variance
Frequency
0.05 0.1 0.15 0.2 0.25 0.3 0.35 0.4 0.45 0.5

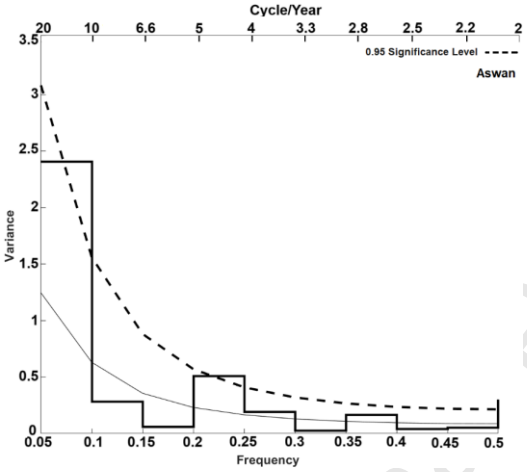
Cycle/Year
20 10 6.6 5 4 3.3 2.8 2.5 2.2 2
0.95 Significance Level
Aswan
Variance
Frequency
0.05 0.1 0.15 0.2 0.25 0.3 0.35 0.4 0.45 0.5

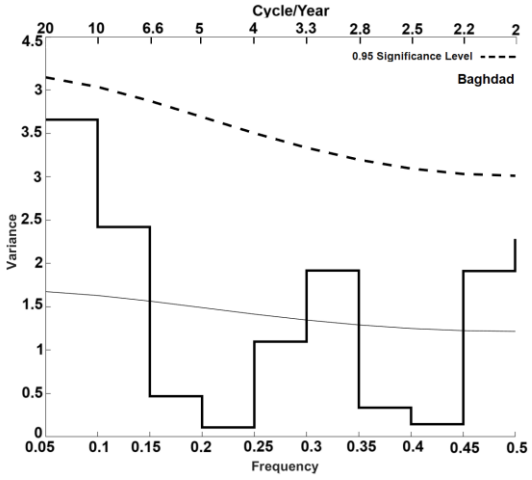
Cycle/Year
20 10 6.6 5 4 3.3 2.8 2.5 2.2 2
0.95 Significance Level
Baghdad
Variance
Frequency
0.05 0.1 0.15 0.2 0.25 0.3 0.35 0.4 0.45 0.5

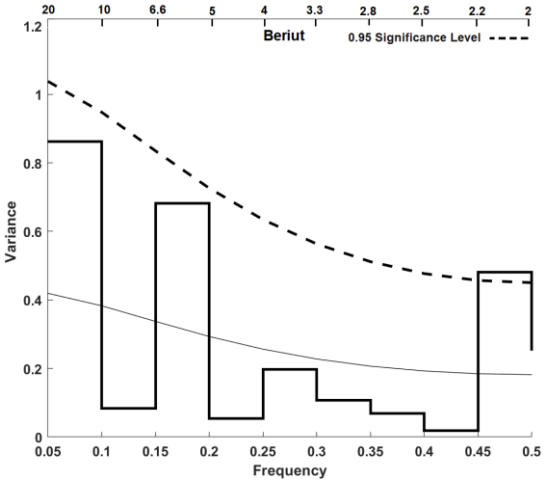
20 10 6.6 5 4 3.3 2.8 2.5 2.2 2
Beriut
0.95 Significance Level
Variance
Frequency
0.05 0.1 0.15 0.2 0.25 0.3 0.35 0.4 0.45 0.5

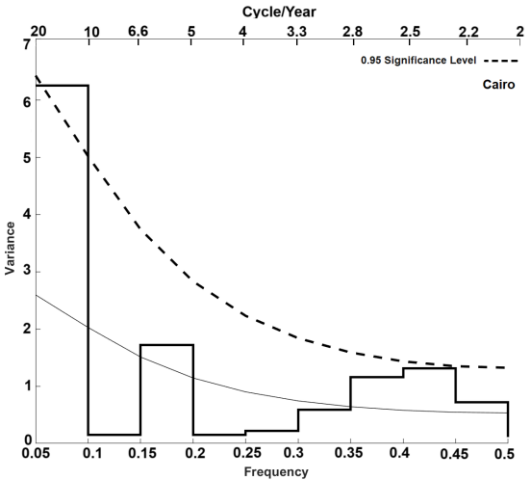
Cycle/Year
20 10 6.6 5 4 3.3 2.8 2.5 2.2 2
0.95 Significance Level
Cairo
Variance
Frequency
0.05 0.1 0.15 0.2 0.25 0.3 0.35 0.4 0.45 0.5

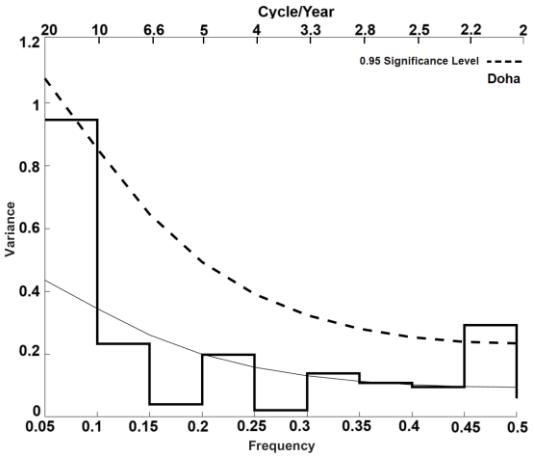
Cycle/Year
20 10 6.6 5 4 3.3 2.8 2.5 2.2 2
0.95 Significance Level
Doha
Variance
Frequency

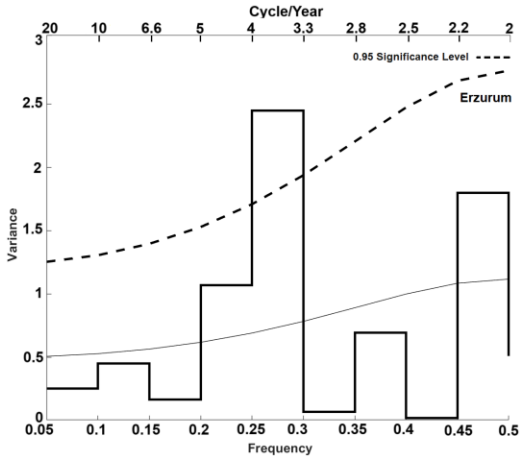
Cycle/Year
20 10 6.6 5 4 3.3 2.8 2.5 2.2 2
0.95 Significance Level
Erzurum
Variance
Frequency

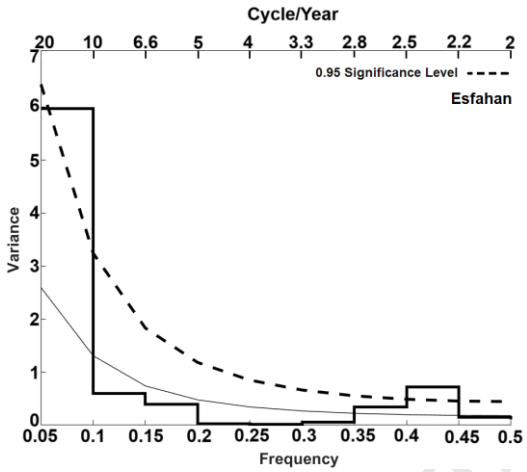
Cycle/Year
20 10 6.6 5 4 3.3 2.8 2.5 2.2 2
0.95 Significance Level
Esfahan
Variance
Frequency

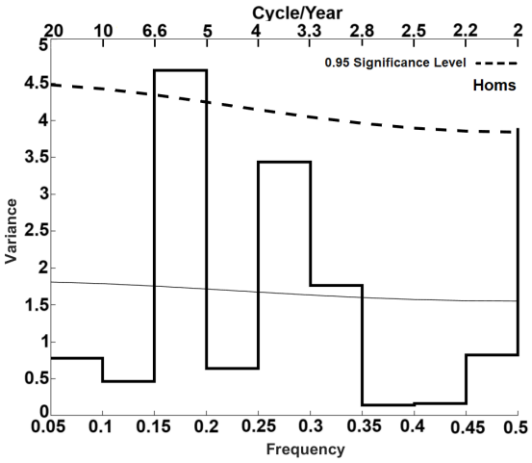
Cycle/Year
20 10 6.6 5 4 3.3 2.8 2.5 2.2 2
0.95 Significance Level
Homs
Variance
Frequency

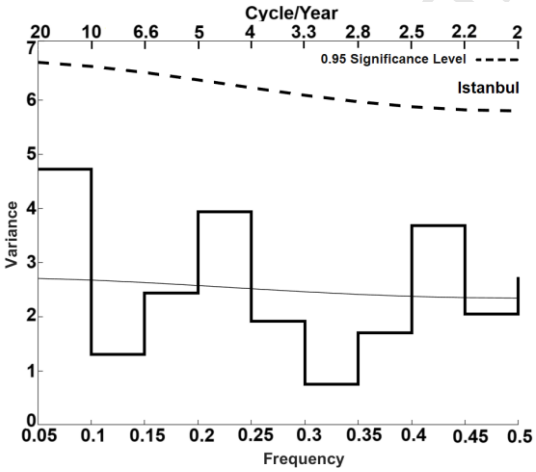
Cycle/Year
20 10 6.6 5 4 3.3 2.8 2.5 2.2 2
0.95 Significance Level
Istanbul
Variance
Frequency

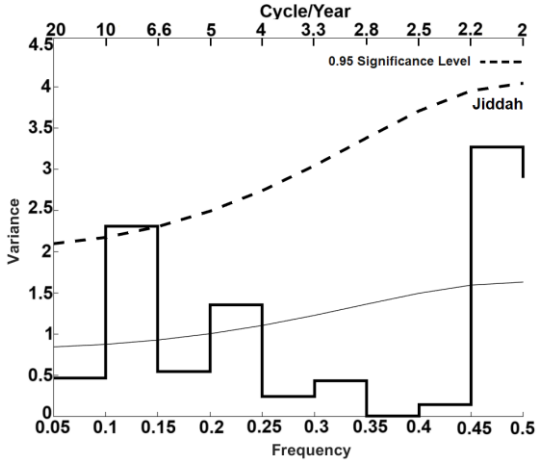
Cycle/Year
20 10 6.6 5 4 3.3 2.8 2.5 2.2 2
0.95 Significance Level
Jiddah
Variance
Frequency

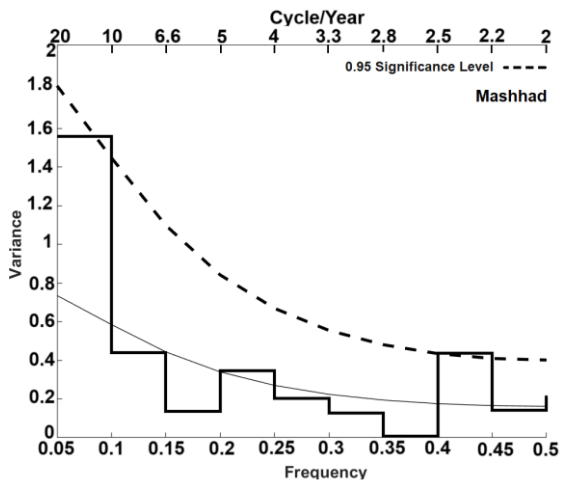
Cycle/Year
20 10 6.6 5 4 3.3 2.8 2.5 2.2 2
0.95 Significance Level
Mashhad
Variance
Frequency
0.05 0.1 0.15 0.2 0.25 0.3 0.35 0.4 0.45 0.5

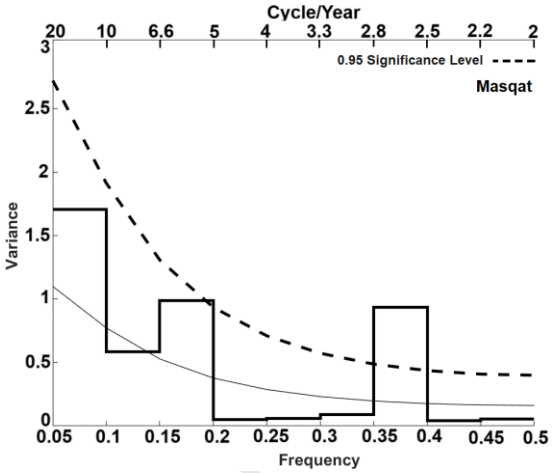
Cycle/Year
20 10 6.6 5 4 3.3 2.8 2.5 2.2 2
0.95 Significance Level
Masqat
Variance
Frequency
0.05 0.1 0.15 0.2 0.25 0.3 0.35 0.4 0.45 0.5

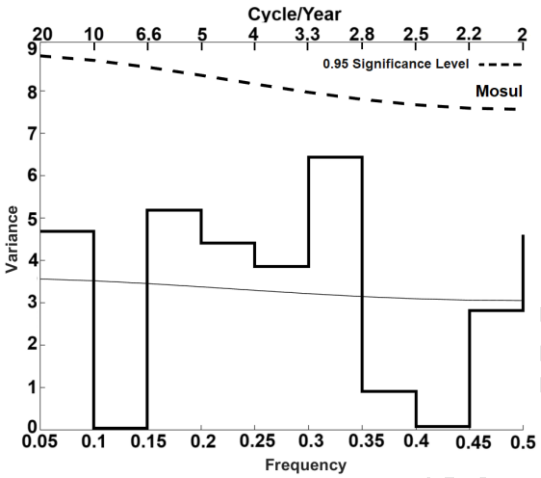
Cycle/Year
20 10 6.6 5 4 3.3 2.8 2.5 2.2 2
0.95 Significance Level
Mosul
Variance
Frequency
0.05 0.1 0.15 0.2 0.25 0.3 0.35 0.4 0.45 0.5

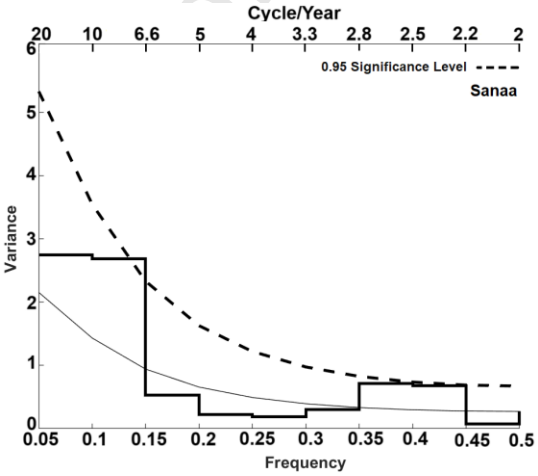
Cycle/Year
20 10 6.6 5 4 3.3 2.8 2.5 2.2 2
0.95 Significance Level
Sanaa
Variance
Frequency
0.05 0.1 0.15 0.2 0.25 0.3 0.35 0.4 0.45 0.5

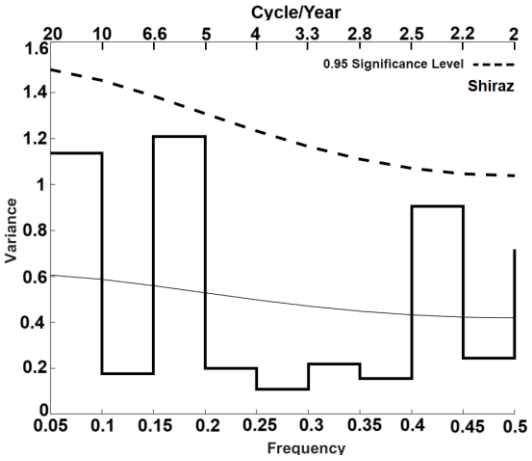
Cycle/Year
20 10 6.6 5 4 3.3 2.8 2.5 2.2 2
0.95 Significance Level
Shiraz
Variance
Frequency
0.05 0.1 0.15 0.2 0.25 0.3 0.35 0.4 0.45 0.5

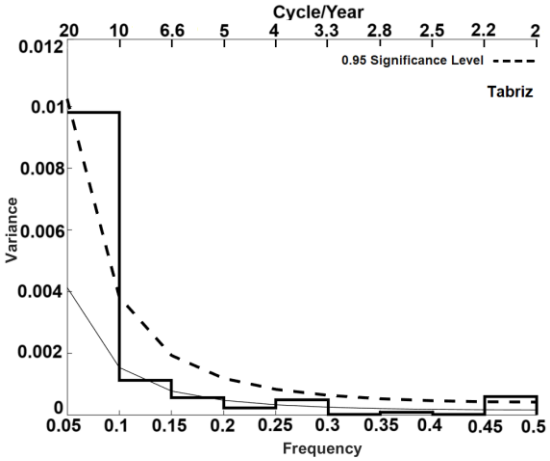
Cycle/Year
20 10 6.6 5 4 3.3 2.8 2.5 2.2 2
0.95 Significance Level
Tabriz
Variance
Frequency
0.05 0.1 0.15 0.2 0.25 0.3 0.35 0.4 0.45 0.5

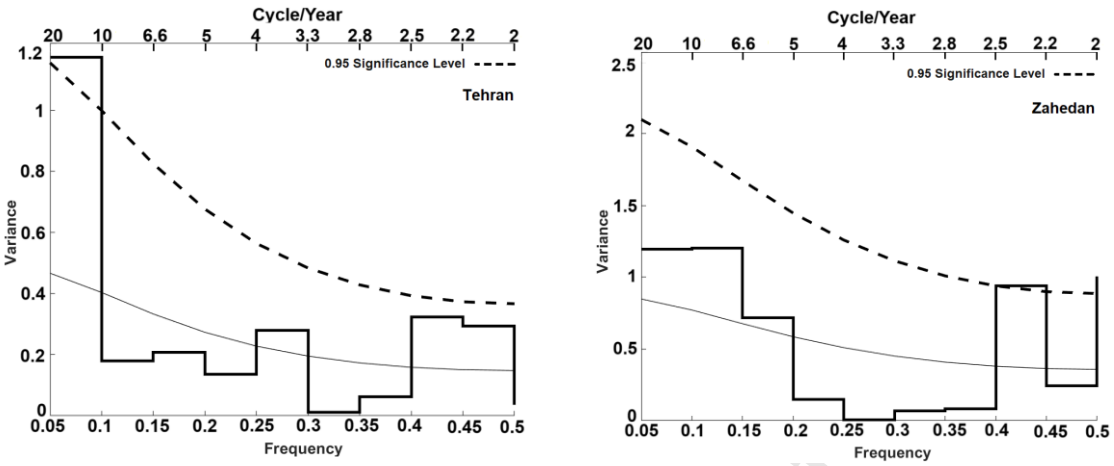

Fig. 10. The periodograms, spectra, and significant boundaries of the TVDI time series in selected pixels

4. Discussion

In this study, the Mann-Kendall (MK) test was employed to analyze drought trends, as it is a widely used method for identifying temporal trends in climatic data. However, the MK test is known to be sensitive to seasonality and serial correlation within the data (Hirsch & Slack, 1984). To overcome this challenge and improve the accuracy of the analysis, the MK test was applied separately for each calendar month. This monthly approach naturally mitigates the effects of seasonality, making the MK test more suitable for detecting changes in this study. By applying the MK test, we more precisely examined seasonal fluctuations in drought trends (Yilmaz, 2019). Additionally, the research employs spectral analysis to identify cyclic drought patterns and investigate their association with large-scale climatic phenomena.

The TVDI trends analysis across the Middle East uncovered distinct spatial and temporal patterns, highlighting the region's complex drought dynamics. Notably, the northern half of the Middle East, including areas in Turkey, Syria, Iraq, western Iran, and eastern Jordan, exhibits prominent upward TVDI trends, particularly during colder months like March and April. These observations indicate an increasing trend in dryness and stress on vegetation in these regions. In contrast, the southern regions, encompassing countries such as Saudi Arabia, Egypt, Oman, and the UAE, show significant downward trends in TVDI, especially during the warmer months (May to September), suggesting improved soil moisture conditions. Seasonal analysis further indicates that northern areas transition from upward to downward trends as winter shifts to spring, while widespread downward trends characterize the summer months across the Middle East. Therefore, the observed trends in the Temperature Vegetation Dryness Index (TVDI) across the Middle East indicate changing climate patterns consistent with previous studies' findings.

For instance, Asakereh et al. (2023) identified significant changes in Iran's precipitation patterns, specifically the shifting of the rainy season. Such a shift has resulted in an alteration in the moisture availability in different months, where traditionally dry months are becoming more humid while some historically wet months are experiencing drier conditions. Our study's detection of significant downward TVDI trends in southern Iran supports these observations, suggesting that shifts in precipitation patterns may directly impact vegetation dryness and drought occurrences. Similarly, the trend patterns observed in the United Arab Emirates are consistent with the findings of Ouarda et al. (2014). Their study indicated a shift in the timing of annual maximum precipitation events across various stations in the country, with peak rainfall now occurring earlier in the winter (December to February) rather than in the later winter months (February to March). Such a seasonal shift may explain the significant upward TVDI trends detected in our analysis for months like March and April, where an earlier end to the rainy season leaves the vegetation more susceptible to dryness during these transitional periods. Such shifts from spring to summer across much of the Middle East suggest that these precipitation timing changes are not isolated seasonal variations but part of a broader regional climatic transformation. The seasonal dynamics of the TVDI trends in our study, characterized by upward trends in higher latitudes during colder months and downward trends during warmer months, appear to be linked to regional climate variations and land-use changes. Previous research has demonstrated that changes in land cover, such as deforestation and agricultural expansion, combined with shifting rainfall patterns, can significantly impact soil moisture and vegetation health (Meher-Homji, 1991). Therefore, the prevalence of significant downward trends during warmer months in countries like Saudi Arabia, Yemen, and the United Arab Emirates may indicate both climatic drivers and human-induced factors contributing to increased aridity. Moreover, the spatial analysis reveals that regions with significant upward TVDI trends, such as northern Middle Eastern areas (northwestern Iran and Turkey), might be experiencing increased dryness and stress on vegetation due to changing precipitation patterns. This observation aligns with studies suggesting that global climate change can have heterogeneous impacts, leading to increased drought conditions in some areas while potentially enhancing vegetation growth in others (Wei et al., 2021).

Understanding the relationship between precipitation patterns and vegetation dryness is crucial for effective water resource management, especially in the arid and semi-arid regions of the Middle East. While the results mainly focus on the temporal and spatial patterns of the Temperature Vegetation Dryness Index (TVDI), exploring how these patterns relate to regional precipitation data provides a more comprehensive view of drought dynamics.

Understanding how precipitation patterns, soil moisture levels, land use, and vegetation indices (such as EVI) correlate with vegetation dryness is essential for managing water resources effectively, particularly in the arid and semi-arid

regions of the Middle East. While our analysis primarily focuses on TVDI's spatial and temporal patterns, examining these patterns about the parameters above provides a more nuanced perspective on drought dynamics.

A comparative analysis using annual precipitation data from the GPM (Global Precipitation Measurement) data and TVDI trends reveals significant spatial patterns in the Middle East. Northern areas, such as Turkey and northern Iran, which have higher annual precipitation (Fig. 11a), show lower TVDI values (Fig. 11b), indicating increased soil moisture and reduced drought severity. This inverse relationship aligns with previous studies showing that increased precipitation enhances soil moisture and reduces dryness (Cong et al., 2017; Du et al., 2023). Conversely, southern and central regions, including the Arabian Peninsula and Egypt, experience lower precipitation levels and higher TVDI values, indicating intensified drought conditions and diminished soil moisture. This observation is consistent with studies on arid climates and water scarcity in these areas (Al Zawad & Aksakal, 2010; Elasha, 2010). These patterns emphasize the need for effective drought mitigation strategies to address the region's vulnerability to climatic variability.

The study shows that the annual average TVDI is affected by the total amount of precipitation and its seasonal and temporal distribution. Regions with moderate annual precipitation may have high TVDI values due to uneven yearly rainfall, causing soil moisture deficits (Koster et al., 2004). These findings suggest that regional climate changes and local factors, such as vegetation cover, influence surface moisture dynamics. Similar patterns are observed outside the Middle East; for example, in Italy, LST and local vegetation changes significantly affect surface dryness (Ghaderpour et al., 2024). Such evidence indicates that regional and global climate changes and local factors are crucial in shaping surface moisture conditions across ecosystems.

The Mann-Kendall trend test indicates that the southern and central regions, such as the Arabian Peninsula, Iraq, and Egypt, exhibit decreasing trends in TVDI, signifying improved soil moisture conditions due to increased precipitation (Fig. 6 and 12b). These results indicate that enhanced rainfall mitigates drought conditions, creating more favorable hydrological environments. Conversely, northern regions, including Turkey and northern Iraq, show increasing TVDI trends, indicating deteriorating drought conditions. Such an increase corresponds to a consistent decrease or lack of change in precipitation in these areas, aligning with previous studies linking reduced rainfall to heightened aridity (Dhorde & Patel, 2016). Regions with no significant trends in TVDI or precipitation are likely influenced by localized factors like soil type, vegetation cover, and topography, which can buffer the impacts of climatic changes (Khosravi et al., 2024). This observation echoes South Asian findings, where regional climate changes and local factors significantly shape surface dryness (Shawky et al., 2023). Sen's slope analysis further confirms that northern regions,

including Turkey and northern Iraq, show positive slopes, indicating worsening drought conditions due to a consistent decrease in precipitation (Fig 9 and 12b).

Conversely, southern regions, like the Arabian Peninsula, exhibit positive slopes in precipitation and a corresponding decrease in TVDI slope, reflecting improved moisture conditions. These findings are supported by recent studies linking increased precipitation in these areas to climatic oscillations (Almazroui, 2020). The findings of this study underscore the need to incorporate both quantitative and temporal precipitation data in TVDI analyses to enhance water resource management and drought mitigation strategies across the Middle East. Adopting a holistic approach that integrates precipitation quantity, seasonal distribution, and soil moisture dynamics can greatly enhance the effectiveness of strategies to mitigate drought impacts. This, in turn, bolsters water security, supports sustainable agricultural practices, and strengthens ecosystem resilience in the region's arid and semi-arid landscapes (World Health Organization, 2019).

Moreover, the study illustrates the effectiveness of combining remote sensing tools, such as GPM and TVDI, for monitoring and predicting drought conditions. This integration facilitates proactive water resource management and enables better-informed agricultural planning. Advanced monitoring techniques are especially critical in the Middle East, where water scarcity presents significant socioeconomic and environmental challenges. By deepening our understanding of drought behavior, these insights can guide the development of effective water management practices, thereby supporting sustainable agriculture and ensuring water security (Dai et al., 2023; Zhang et al., 2011).

A spatial comparison between the soil moisture map (Fig. 13a) and the Middle East's annual average TVDI (Fig. 11b) reveals critical information regarding the region's water dynamics and drought patterns. Areas exhibiting elevated soil moisture levels, particularly in the northern Middle East, including Turkey, upper Iraq, and portions of northern Iran, consistently demonstrate lower annual TVDI readings (Fig. 11b). This correlation underscores these regions' superior capacity to maintain soil moisture, suggesting that abundant vegetation, encompassing forests and agricultural lands, significantly enhances water retention in the soil and mitigates drought intensity. These zones, characterized by higher precipitation and more favorable climate conditions, exhibit an increased capacity to absorb and retain water, directly contributing to lower TVDI measurements. Furthermore, topographical factors such as elevation and proximity to water sources can influence soil moisture patterns in these regions.

Land use and TVDI maps (Fig. 1b) further confirm that the northern Middle East, including Turkey, northern Iraq, and parts of Iran, generally exhibits lower TVDI values due to dense vegetation cover, such as trees and crops, which indicate better moisture conditions and reduced drought severity (Fathi-Taperasht et al., 2023). Agricultural lands and

rangelands also tend to have lower TVDI values, attributed to their vegetation's ability to retain moisture, resulting in greater drought resilience (Martin-Sotoca et al., 2023). In contrast, the southern and central regions of the Middle East, such as the Arabian Peninsula and Egypt, predominantly consist of bare ground and rangeland, displaying higher TVDI values, which reflect more severe dryness and reduced soil moisture (Sahour et al., 2020). The lack of sufficient vegetation cover in these areas diminishes their capacity to retain soil moisture, increasing their susceptibility to moisture fluctuations. Bare lands and urban areas, due to their impermeable surfaces and absence of vegetation, also exhibit high TVDI values, indicating greater dryness and heightened vulnerability to drought.

Building on the insights from soil moisture and land use patterns, the relationship between vegetation density and drought intensity was further examined using the Enhanced Vegetation Index (EVI) (Fig. 13b). This approach highlights that areas with denser vegetation cover, particularly in the northern Middle East, including regions such as Turkey, northern Iraq, and parts of northern Iran, exhibit higher EVI values. These regions, primarily consisting of forests and agricultural lands, show lower Temperature Vegetation Dryness Index (TVDI) values, which signify reduced drought severity and improved moisture conditions. This pattern underscores the positive impact of vegetation cover on soil moisture retention and drought mitigation, a role previously highlighted in studies focused on moisture balance maintenance (García-Leoz et al., 2018; He et al., 2024).

In contrast, areas such as the Arabian Peninsula and parts of southern Iraq, Yemen, Oman, and Egypt, with sparse vegetation and lower EVI values, correspond with higher TVDI values, reflecting more severe dryness and reduced soil moisture retention. The absence of sufficient vegetation in these regions not only limits their ability to retain soil moisture but also heightens their sensitivity to climatic variability and moisture fluctuations, further stressing the critical role of vegetation in stabilizing soil moisture and mitigating drought impacts (Li et al., 2022).

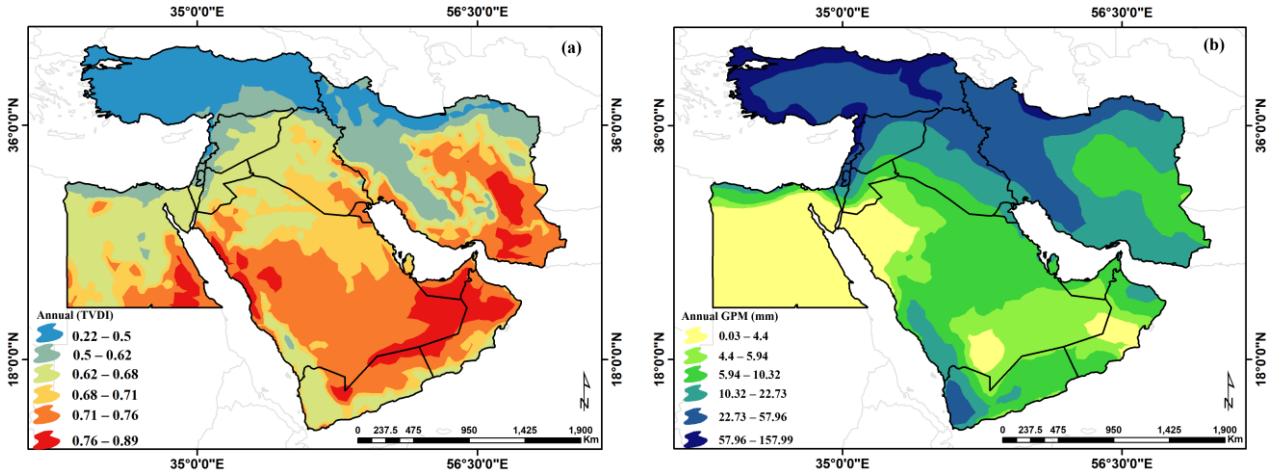

Fig. 11. Spatial distribution of annual TVDI (a) and annual precipitation (b) in the Middle East

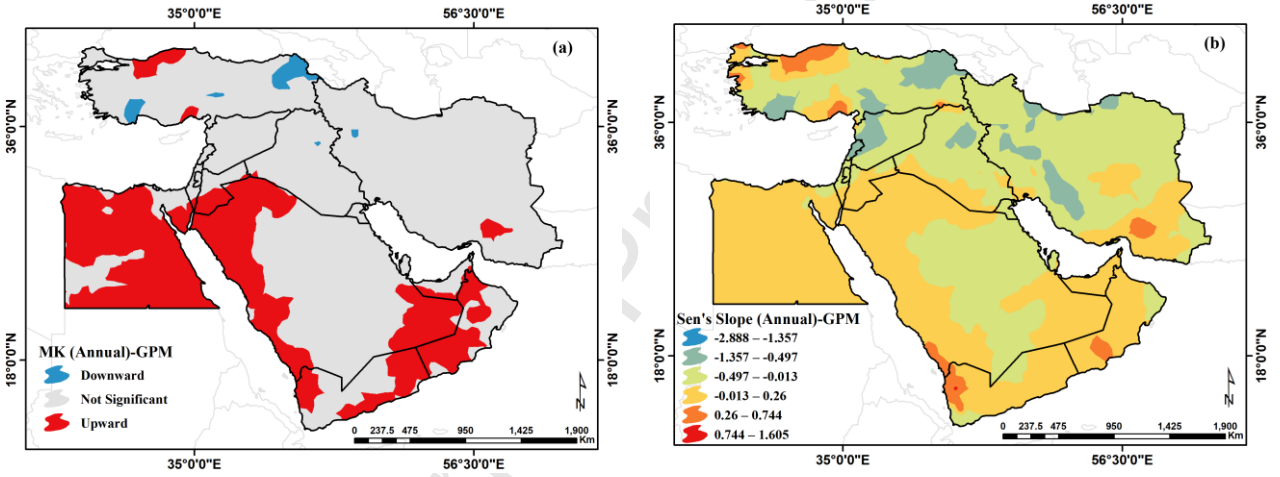

Fig. 12. Spatial distribution of the annual TVDI trend (a) and its slope changes (b) in the Middle East

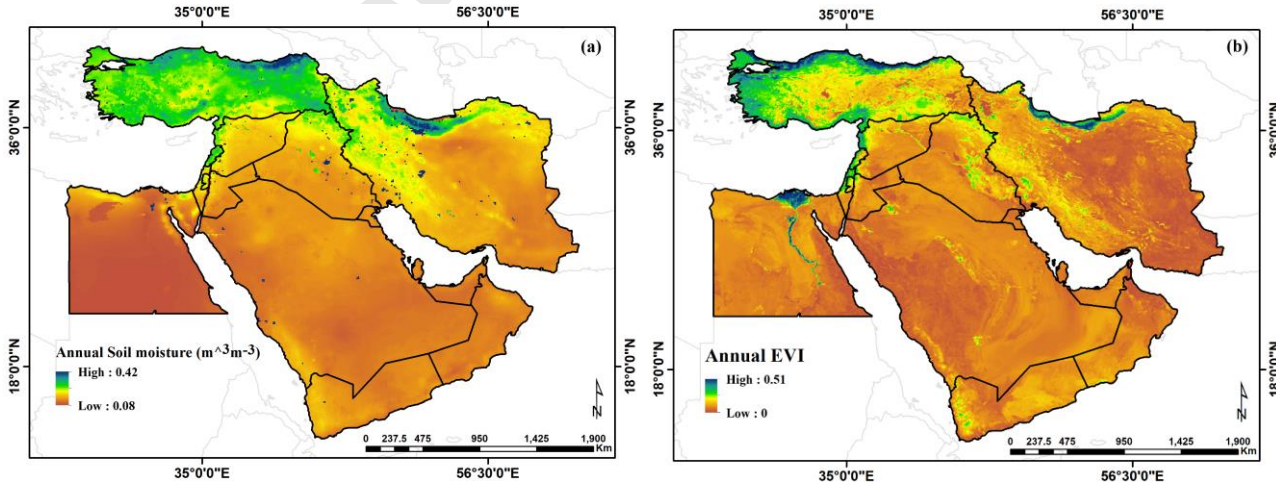

Fig. 13. Spatial distribution of annual soil moisture (a) and EVI (b) in the Middle East.

A careful examination of the spatial distribution of TVDI cycles across the Middle East revealed inter-annual fluctuations in TVDI values with varying return periods (Fig. 13). The data in the table corroborate that the 2-3-year cycles significantly influence TVDI values within the Middle East, encompassing more than 68.77% of the study area. This cycle exhibits a widespread presence in countries such as Iran, Oman, Yemen, and Turkey, as well as the southern regions of Saudi Arabia and Egypt. Numerous researchers have linked these cycles to phenomena like the El Niño-Southern Oscillation (ENSO) and the Quasi-Biennial Oscillation (QBO), which are present in large-scale atmospheric circulation patterns. For example, Selvam and Joshi (1995) identified a linkage between the 2-3-year variations and surface temperature and (Lamb, 1972) correlated these 2-3-year cycles with rainfall patterns in northwestern Iran, attributing them to the Quasi-Biennial Oscillation (QBO). Recent studies, such as (Niranjan Kumar & Ouarda, 2014), have explored how ENSO modulates the precipitation variability in the United Arab Emirates and surrounding regions, revealing significant teleconnections between UAE precipitation and global sea surface temperatures (SSTs). The shift of the subtropical jet stream (STJ) due to ENSO-related Rossby wave propagation is a key factor influencing regional weather patterns. This is consistent with the findings in our study, where ENSO plays a crucial role in shaping the drought cycles observed across the Middle East.

Similarly, (Niranjan Kumar et al., 2016) emphasized the impact of Rossby waves on precipitation variability in the Arabian Peninsula, further supporting the connection between large-scale atmospheric phenomena and regional climate patterns. In South Asia, Shawky et al. (2023) identified similar patterns of increasing and decreasing LST influenced by atmospheric oscillations such as ENSO, reinforcing the connection between seasonal variations in LST and large-scale climate changes. Alongside the prevalent 2-3-year cycle, there is evidence of a 4-year cycle in the region, which many researchers attribute to the ENSO phenomenon.

Azad et al. (2010) ascribed the 3-5-year cycles to seasonal rainfall patterns in India, citing their connection to the ENSO phenomenon. Similarly, (Kalayci et al., 2004) linked the 2-6-year cycles with precipitation occurrences in Turkey, specifically associating them with El Niño. Furthermore (Asakereh & Razmi, 2012b) provided evidence of the significant impact of 3-5-year cycles on precipitation in northwestern Iran, attributing them to the ENSO phenomenon. According to Fig. 11, these cycles are discernible in the northern and southern regions of Iran, in eastern Oman and eastern areas of Turkey, and sporadically in smaller regions within central Saudi Arabia. In the central parts of the Middle East (Saudi Arabia, Iraq, and Egypt), 7-15-year cycles are evident. The presence of cycles with these return periods is commonly attributed to solar activity by many researchers, such as Mitchell Jr et al. (1979) and Jahanbakhsh and Edalatdoust (2008). Furthermore, non-sinusoidal cycles with return periods matching the length of

the statistical period are observable in the same geographical areas, albeit with smaller spatial coverage. These cycles are associated with underlying trends in the data.

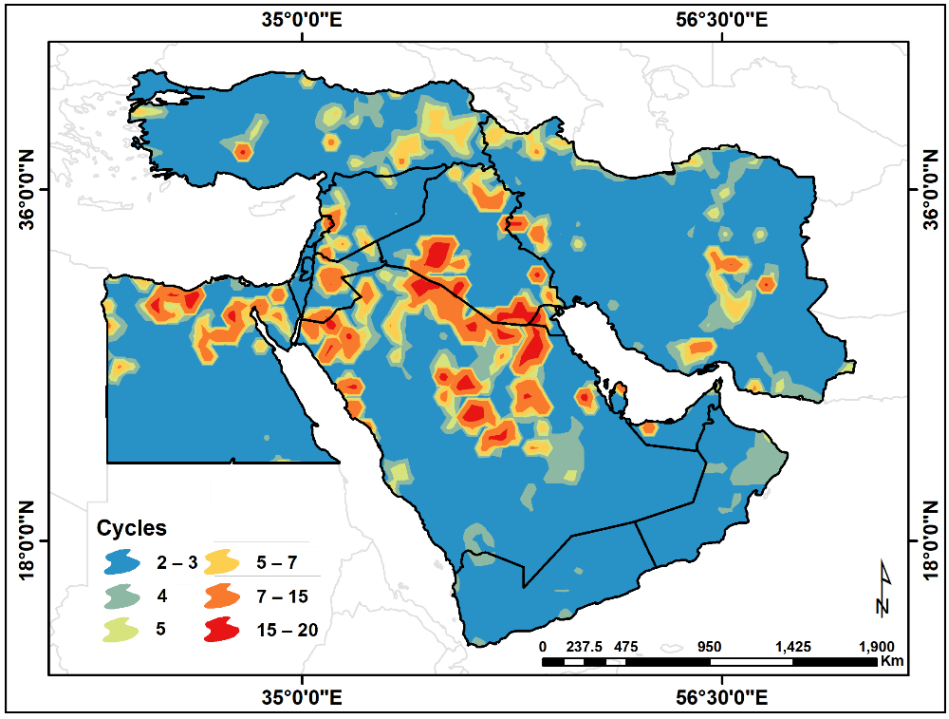

Fig. 13. Spatial Distribution of TVDI Cycles in the Middle East

5. Conclusions

The TVDI, which integrates data from the NDVI and LST, provides a comprehensive method for analyzing soil moisture levels across terrestrial landscapes. Due to its ability to offer a detailed perspective on drought conditions, the TVDI index has gained widespread recognition and is extensively used in various ecosystems worldwide. It is an indispensable tool for monitoring and assessing aridity and drought patterns.

This study aimed to analyze the trends and spectral characteristics of TVDI for 258,087 pixels across the Middle East, covering the period from 2003 to 2022. According to the Mann-Kendall test, significant upward trends in TVDI are most prominent in March and April, while September shows the least significant upward trend. This seasonal variation reflects the influence of temperature and precipitation on vegetation dynamics. Notably, upward TVDI trends are more prevalent in the northern half of the Middle East, whereas the southern half experiences significant downward trends, particularly during the warmer months.

A seasonal analysis reveals that winter generally lacks significant TVDI trends, whereas spring and summer exhibit notable downward trends, especially in the southern and western regions. The annual trend map suggests a long-term declining trend in TVDI for most latitudinal bands. The steepest upward TVDI slope values occur during the warmer

months, with April showing the highest slope. Conversely, the downward trend slopes are steepest in July, indicating increased dryness.

Spatially, significant downward slope values are concentrated in the southern and western regions of the Middle East. The seasonal slope analysis further reveals that the most pronounced upward slope values align with the spring season, while the most significant downward slopes occur during the warmer months. The annual slope maps divide the region into two segments: the southern, eastern, and western Middle East exhibit negative slopes, while the central and northern regions display positive slope trends, except for western Turkey. Furthermore, comparing GPM data with TVDI trends revealed a clear connection between precipitation and drought conditions in the region. In northern areas such as Turkey and northern Iran, which receive more rainfall, lower TVDI values are generally observed, indicating better soil moisture and less severe droughts. In contrast, southern and central regions, including the Arabian Peninsula and Egypt, exhibit higher TVDI values due to lower rainfall, signifying more intense drought conditions. These findings highlight the need for targeted drought mitigation strategies to address the region's sensitivity to changing climate patterns.

In the second phase, periodograms of TVDI time series were plotted for 26 individual stations to assess the significance of cycles at a 95% confidence level. Most stations observed significant cycles, indicating the emergence of specific patterns and coherent TVDI values in cyclic behavior. However, certain stations, including Al Basra, Al Riyadh, Baghdad, Istanbul, Mosul, and Shiraz, did not display distinct cycles, suggesting random behavior. Non-sinusoidal cycles with a return period equal to the length of the statistical period were evident at stations such as Adana, Al Kuwayt, Al Madinah, Amman, Cairo, and Tehran. A significant first harmonic in these periodograms indicated a trend within the data.

The spatial distribution of TVDI cycles across the Middle East revealed inter-annual fluctuations with varying return periods. The most prominent cycle, with a 2-3-year return period, was observed in over 68.77% of the study area, including Iran, Oman, Yemen, Turkey, and the southern regions of Saudi Arabia and Egypt. This cycle has been associated with large-scale atmospheric phenomena such as the El Niño-Southern Oscillation (ENSO) and the Quasi-Biennial Oscillation (QBO). Additionally, a 4-year cycle was linked to ENSO activity in the region. Cycles with 7 to 15 years return periods were observed in central parts of the Middle East, attributed to solar activity. Non-sinusoidal cycles matching the length of the statistical period were also found in various geographical areas, suggesting underlying trends in the TVDI data.

CRediT authorship contribution statement

Younes Khosravi: Methodology, Software, Writing – original draft, Writing – review & editing. **Saeid Homayouni**: Methodology, Investigation, Writing – original draft, Writing – review & editing. **Taha Ouarda**: Supervise, methodology, writing – review & editing, conceptualization.

Ethics approval

Not applicable.

Consent to participate

Not applicable.

Consent for publication

Not applicable.

Declaration of competing interest

The authors declare that they have no known competing financial interests or personal relationships that could have appeared to influence the work reported in this paper.

Funding

This research is financially supported by the National Sciences and Engineering Research Council of Canada (NSERC) (funding number: RGPIN-2024-06736). The authors wish to express their appreciation to Pr. XXXXXXXX, Editor, and two anonymous reviewers for their invaluable comments and suggestions, which helped improve the quality of the paper.

Acknowledgments

We would like to thank Prof. Hossein Asakereh for his assistance with the spectral analysis coding.

Data Availability

The dataset and the codes used for this analysis are available at http://drive.google.com/file/d/1ymTQj6DrFHzu7oFjd_4Ee8HETUI6xZJG/view. Ensuring the reproducibility, transparency, and accessibility of scientific findings is essential to advance sustainable science and foster a collaborative digital society, as highlighted by Huettmann and Arhonditsis (2023). This open-access approach allows for the sharing of resources for the broader benefit of the research community.

References

Agrawala, S., Barlow, M., Cullen, H., & Lyon, B., 2001. The drought and humanitarian crisis in central and southwest Asia: A climate perspective.

Ahani, H., Kherad, M., Kousari, M. R., Rezaeian-Zadeh, M., Karampour, M. A., Ejraee, F., & Kamali, S., 2012. An investigation of trends in precipitation volume for the last three decades in different regions of Fars province, Iran. Theoretical and Applied Climatology, 109(3-4), 361-382.

Al-Qinna, M. I., Hammouri, N. A., Obeidat, M. M., & Ahmad, F. Y., 2011. Drought analysis in Jordan under current and future climates. Climatic Change, 106(3), 421-440.

Al Zawad, F. M., & Aksakal, A., 2010. Impacts of climate change on water resources in Saudi Arabia. Global warming: engineering solutions, 511-523.

Ali, M. G., Younes, K., Esmaeil, A., & Fatemeh, T., 2011. Assessment of geostatistical methods for spatial analysis of SPI and EDI drought indices. World Applied Sciences Journal, 15(4), 474-482.

Almazroui, M., 2020. Rainfall trends and extremes in Saudi Arabia in recent decades. Atmosphere, 11(9), 964.

Asakereh, H., Doostkamian, M., & Qaemi, H., 2014. Analysis of anomalies and perceptible water cycles in Iran atmosphere. Physical Geography Research Quarterly, 46(4), 435-444.

Asakereh, H., Doostkamian, M., & Sadrafshary, S., 2015. Anomalies and cycles of precipitable water over Iran in recent decades. Arabian Journal of Geosciences, 8(11), 9569-9576.

Asakereh, H., Masoodian, S. A., & Tarkarani, F., 2023. Identification of Iran's precipitation regimes. Theoretical and Applied Climatology, 1-16.

Asakereh, H., & Razmi, R., 2012a. Analysis of annual precipitation changes in northwest of Iran.

Asakereh, H., & Razmi, R., 2012b. Analysis of Annual Precipitation Changes in Northwest of Iran. Geography and Environmental Planning, 23(3), 147-162.

Azad, S., Vignesh, T., & Narasimha, R., 2010. Periodicities in Indian monsoon rainfall over spectrally homogeneous regions. International journal of climatology, 30(15), 2289-2298.

Barlow, M., Zaitchik, B., Paz, S., Black, E., Evans, J., & Hoell, A., 2016. A review of drought in the Middle East and southwest Asia. Journal of climate, 29(23), 8547-8574.

Basha, G., Marpu, P. R., & Ouarda, T. B., 2015. Tropospheric temperature climatology and trends observed over the Middle East. Journal of Atmospheric and Solar-Terrestrial Physics, 133, 79-86.

Basha, G., Ouarda, T. B., & Marpu, P. R., 2015. Long-term projections of temperature, precipitation and soil moisture using non-stationary oscillation processes over the UAE region. International journal of climatology, 35(15).

Behifar, M., Kakroodi, A. A., Kiavarz, M., & Azizi, G., 2023. Satellite-based drought monitoring using optimal indices for diverse climates and land types. Ecological Informatics, 76, 102143.

Bhalme, H. N., & Mooley, D. A., 1980. Large-scale droughts/floods and monsoon circulation.

Bian, Z., Roujean, J., Fan, T., Dong, Y., Hu, T., Cao, B., Li, H., Du, Y., Xiao, Q., & Liu, Q., 2023. An angular normalization method for temperature vegetation dryness index (TVDI) in monitoring agricultural drought. Remote Sensing of environment, 284, 113330.

Byun, H.-R., & Wilhite, D. A., 1999. Objective quantification of drought severity and duration. Journal of climate, 12(9), 2747-2756.

Carlson, T. N., Perry, E. M., & Schmugge, T. J., 1990. Remote estimation of soil moisture availability and fractional vegetation cover for agricultural fields. Agricultural and Forest Meteorology, 52(1-2), 45-69.

Chaerle, L., & Van Der Straeten, D., 2000. Imaging techniques and the early detection of plant stress. Trends in plant science, 5(11), 495-501.

Chandran, A., Basha, G., & Ouarda, T., 2016. Influence of climate oscillations on temperature and precipitation over the United Arab Emirates. International journal of climatology, 36(1), 225-235.

Chatfield, C., 2013. The analysis of time series: theory and practice. Springer.

Chen, C., Zhao, S., Duan, Z., & Qin, Z., 2015. An improved spatial downscaling procedure for TRMM 3B43 precipitation product using geographically weighted regression. IEEE Journal of Selected Topics in Applied Earth Observations and Remote Sensing, 8(9), 4592-4604.

Chen, J., Yang, H., Jin, T., & Wu, K., 2024. Assessment of terrestrial ecosystem sensitivity to climate change in arid, semi-arid, sub-humid, and humid regions using EVI, LAI, and SIF products. Ecological Indicators, 158, 111511.

Christian, J. I., Basara, J. B., Hunt, E. D., Otkin, J. A., & Xiao, X., 2020. Flash drought development and cascading impacts associated with the 2010 Russian heatwave. Environmental Research Letters, 15(9), 094078.

Cong, D., Zhao, S., Chen, C., & Duan, Z., 2017. Characterization of droughts during 2001–2014 based on remote sensing: a case study of Northeast China. Ecological Informatics, 39, 56-67.

Croitoru, L., & Liagre, L., 2013. Contribution of forests to a green economy in the Middle East and North Africa region. Forêt Méditerranéenne, 34(4), 291-298.

da Silva, V. d. P. R., 2004. On climate variability in Northeast of Brazil. Journal of Arid Environments, 58(4), 575-596.

Dai, A., 2011. Drought under global warming: a review. Wiley Interdisciplinary Reviews: Climate Change, 2(1), 45-65.

Dai, R., Chen, S., Cao, Y., Zhang, Y., & Xu, X., 2023. A Modified Temperature Vegetation Dryness Index (mTVDI) for agricultural drought assessment based on MODIS Data: A case study in Northeast China. Remote Sensing, 15(7), 1915.

De Chatel, F., 2017. Water sheikhs and dam builders: Stories of people and water in the Middle East. Routledge.

De Châtel, F., 2007. Perceptions of water in the Middle East: the role of religion, politics and technology in concealing the growing water scarcity. Water Resources in the Middle East: Israel-Palestinian Water Issues—From Conflict to Cooperation, 53-60.

Demirgül, T., Yılmaz, C. B., Zıpır, B. N., Kart, F. S., Pehriz, M. F., Demir, V., & Sevimli, M. F., 2022. Investigation of Turkey's climate periods in terms of precipitation and temperature changes. Engineering Applications, 1(1), 80-90.

Dhorde, A., & Patel, N., 2016. Spatio-temporal variation in terminal drought over western India using dryness index derived from long-term MODIS data. Ecological Informatics, 32, 28-38.

Dorvlo, A. S., & Ampratwum, D. B., 2000. Harmonic analysis of global irradiation. Renewable Energy, 20(4), 435-443.

Du, L., Song, N., Liu, K., Hou, J., Hu, Y., Zhu, Y., Wang, X., Wang, L., & Guo, Y., 2017. Comparison of two simulation methods of the temperature vegetation dryness index (TVDI) for drought monitoring in semi-arid regions of China. Remote Sensing, 9(2), 177.

Du, M., Huang, S., Leng, G., Huang, Q., Guo, Y., & Jiang, J., 2023. Multi-timescale-based precipitation concentration dynamics and their asymmetric impacts on dry and wet conditions in a changing environment. Atmospheric Research, 291, 106821.

Ehrlich, D., & Lambin, E. F., 1996. Broad scale land-cover classification and interannual climatic variability. Int. J. Remote Sens., 17, 845–862.

Elasha, B. O., 2010. Mapping of climate change threats and human development impacts in the Arab region. UNDP Arab Development Report–Research Paper Series, UNDP Regiona Bureau for the Arab States.

Fallahchai, M. M., 2011. A diversity survey of mountainous forests trees in north of Iran. Advances in Environmental Biology, 3207-3212.

Fathi-Taperasht, A., Shafizadeh-Moghadam, H., Sadian, A., Xu, T., & Nikoo, M. R., 2023. Drought-induced vulnerability and resilience of different land use types using time series of MODIS-based indices. International Journal of Disaster Risk Reduction, 91, 103703.

Fetene, Z. A., Weldegerima, T. M., Zeleke, T. T., & Nigussie, M., 2018. Harmonic analysis of precipitation time series in Lake Tana Basin, Ethiopia. Advances in Meteorology, 2018.

Fiala, T., Ouarda, T. B., & Hladný, J., 2010. Evolution of low flows in the Czech Republic. Journal of Hydrology, 393(3-4), 206-218.

Ganguly, N. D., 2016. Atmospheric changes observed during April 2015 Nepal earthquake. Journal of Atmospheric and Solar-Terrestrial Physics, 140, 16-22.

García-Leoz, V., Villegas, J. C., Suescún, D., Flórez, C. P., Merino-Martín, L., Betancur, T., & León, J. D., 2018. Land cover effects on water balance partitioning in the Colombian Andes: improved water availability in early stages of natural vegetation recovery. Regional Environmental Change, 18, 1117-1129.

Gebremicael, T. G., Mohamed, Y. A., & Hagos, E. Y., 2017. Temporal and spatial changes of rainfall and streamflow in the Upper Tekezē–Atbara river basin, Ethiopia. Hydrology and Earth System Sciences, 21(4), 2127-2142.

Gerhards, M., Schlerf, M., Mallick, K., & Udelhoven, T., 2019. Challenges and future perspectives of multi-/Hyperspectral thermal infrared remote sensing for crop water-stress detection: A review. Remote Sensing, 11(10), 1240.

Gerken, T., Bromley, G. T., Ruddell, B. L., Williams, S., & Stoy, P. C., 2018. Convective suppression before and during the United States Northern Great Plains flash drought of 2017. Hydrology and Earth System Sciences, 22(8), 4155-4163.

Ghaderpour, E., Mazzanti, P., Bozzano, F., & Scarascia Mugnozza, G., 2024. Trend Analysis of MODIS Land Surface Temperature and Land Cover in Central Italy. Land, 13(6), 796.

Ghaemi, H., Asakereh, H., & Rezaei, S., 2017. Spectral Analysis of annual average of red sea low pressure during 1330-1389. Geographic Thought, 8(15), 139-150.

Ghaleb, F., Mario, M., & Sandra, A. N., 2015. Regional landsat-based drought monitoring from 1982 to 2014. Climate, 3(3), 563-577.

Ghozat, A., Sharafati, A., & Hosseini, S. A., 2022. Satellite-based monitoring of meteorological drought over different regions of Iran: application of the CHIRPS precipitation product. Environmental Science and Pollution Research, 29(24), 36115-36132.

Gonzalez, R., Ouarda, T., Marpu, P., Allam, M., Eltahir, E., & Pearson, S. (2016). Water budget analysis in arid regions, application to the United Arab Emirates. Water, 8, 415. In.

Guo, Y., Han, L., Zhang, D., Sun, G., Fan, J., & Ren, X., 2023. The Factors Affecting the Quality of the Temperature Vegetation Dryness Index (TVDI) and the Spatial–Temporal Variations in Drought from 2011 to 2020 in Regions Affected by Climate Change. Sustainability, 15(14), 11350.

Hamdi, Y., Charron, C., & Ouarda, T. B., 2021. A non-stationary heat spell frequency, intensity, and duration model for France, integrating teleconnection patterns and climate change. Atmosphere, 12(11), 1387.

Hamdi, Y., Chebana, F., & Ouarda, T. B., 2016. Bivariate drought frequency analysis in the Medjerda River Basin, Tunisia. Journal of Civil and Environmental Engineering, 6(3).

Hameed, M., Ahmadalipour, A., & Moradkhani, H., 2020. Drought and food security in the middle east: An analytical framework. Agricultural and Forest Meteorology, 281, 107816.

Hao, C., Zhang, J., & Yao, F., 2015. Combination of multi-sensor remote sensing data for drought monitoring over Southwest China. International Journal of Applied Earth Observation and Geoinformation, 35, 270-283.

He, S., Zhang, C., Meng, F.-R., Bourque, C. P.-A., Huang, Z., & Li, X., 2024. Impacts of re-vegetation on soil water dynamics in a semiarid region of Northwest China. Science of The Total Environment, 911, 168496.

Hirsch, R. M., Helsel, D. R., Cohn, T. A., & Gilroy, E. J., 1992. Statistical analysis of hydrologic data. Handbook of hydrology., 17-55.

Hirsch, R. M., & Slack, J. R., 1984. A nonparametric trend test for seasonal data with serial dependence. Water Resources Research, 20(6), 727-732.

Horn, L. H., & Bryson, R. A., 1960. Harmonic analysis of the annual March of precipitation over the United States 1. Annals of the Association of American Geographers, 50(2), 157-171.

Huete, A., Didan, K., Miura, T., Rodriguez, E. P., Gao, X., & Ferreira, L. G., 2002. Overview of the radiometric and biophysical performance of the MODIS vegetation indices. Remote Sensing of Environment, 83(1-2), 195-213.

Huete, A., Justice, C., & Van Leeuwen, W., 1999. MODIS vegetation index (MOD13). Algorithm theoretical basis document, 3(213), 295-309.

Huettmann, F., & Arhonditsis, G., 2023. Towards an ecological informatics scholarship that is reflective, repeatable, transparent, and sharable! Ecological Informatics, 76, 102132.

Immerzeel, W., Quiroz, R., & De Jong, S., 2005. Understanding precipitation patterns and land use interaction in Tibet using harmonic analysis of SPOT VGT-S10 NDVI time series. International journal of remote sensing, 26(11), 2281-2296.

Jahanbakhsh, S., & Edalatdoust, M., 2008. The effect of solar activity on the variation of annual precipitation in Iran.

Kafle, H. K., & Bruins, H. J., 2009. Climatic trends in Israel 1970–2002: warmer and increasing aridity inland. Climatic Change, 96(1-2), 63-77.

Kalayci, S., Karabörk, M., & Kahya, E., 2004. Analysis of El Nino signals on Turkish streamflow and precipitation patterns using spectral analysis. Fresenius Environmental Bulletin, 13(8), 719-725.

Kaniewski, D., Van Campo, E., & Weiss, H., 2012. Drought is a recurring challenge in the Middle East. Proceedings of the National Academy of Sciences, 109(10), 3862-3867.

Karabörk, M. Ç., 2007. Trends in drought patterns of Turkey. Journal of Environmental Engineering and Science, 6(1), 45-52.

Karakani, E. G., Malekian, A., Gholami, S., & Liu, J., 2021. Spatiotemporal monitoring and change detection of vegetation cover for drought management in the Middle East. Theoretical and Applied Climatology, 144, 299-315.

Kendall, M. G., 1975. Rank correlation methods. Griffin, London. Kendall MG.

Khanmohammadi, N., Rezaie, H., & Behmanesh, J., 2022. Investigation of drought trend on the basis of the best obtained drought index. Water resources management, 36(4), 1355-1375.

Khosravi, Y., & Abbasi, E., 2016. Spatial analysis of environmental data with geostatistics. Zanjan, Azarkalak.

Khosravi, Y., Homayouni, S., & St-Hilaire, A., 2024. An integrated dryness index based on geographically weighted regression and satellite earth observations. Science of The Total Environment, 911, 168807.

Kirkyla, K. I., & Hameed, S., 1989. Harmonic analysis of the seasonal cycle in precipitation over the United States: A comparison between observations and a general circulation model. Journal of climate, 2(12), 1463-1475.

Klisch, A., & Atzberger, C., 2016. Operational drought monitoring in Kenya using MODIS NDVI time series. Remote Sensing, 8(4), 267.

Kogan, F. N., 1995. Droughts of the late 1980s in the United States as derived from NOAA polar-orbiting satellite data. Bulletin of the American Meteorological Society, 76(5), 655-668.

Koster, R. D., Dirmeyer, P. A., Guo, Z., Bonan, G., Chan, E., Cox, P., Gordon, C., Kanae, S., Kowalczyk, E., & Lawrence, D., 2004. Regions of strong coupling between soil moisture and precipitation. Science, 305(5687), 1138-1140.

Lamb, H. H., 1972. Fundamentals and climate now (Vol. 1). Psychology Press.

Laz, O. U., Rahman, A., & Ouarda, T. B., 2023a. Compound heatwave and drought hotspots and their trends in Southeast Australia. Natural Hazards, 1-30.

Laz, O. U., Rahman, A., & Ouarda, T. B., 2023b. Compound heatwave and drought hotspots and their trends in Southeast Australia. Natural Hazards, 119(1), 357-386.

Lazzarini, M., Molini, A., Marpu, P. R., Ouarda, T. B., & Ghedira, H., 2015. Urban climate modifications in hot desert cities: The role of land cover, local climate, and seasonality. Geophysical Research Letters, 42(22), 9980-9989.

Lee, J. H., & Julien, P. Y., 2017. Influence of the El Niño/southern oscillation on South Korean streamflow variability. Hydrological Processes, 31(12), 2162-2178.

Li, S., Yao, Z., Liu, Z., Wang, R., Liu, M., & Adam, J. C., 2019. The spatio-temporal characteristics of drought across Tibet, China: derived from meteorological and agricultural drought indexes. Theoretical and Applied Climatology, 137, 2409-2424.

Li, W., Migliavacca, M., Forkel, M., Denissen, J. M., Reichstein, M., Yang, H., Duveiller, G., Weber, U., & Orth, R., 2022. Widespread increasing vegetation sensitivity to soil moisture. Nature Communications, 13(1), 3959.

Li, Z., Wang, Y., Zhou, Q., Wu, J., Peng, J., & Chang, H., 2008. Spatiotemporal variability of land surface moisture based on vegetation and temperature characteristics in Northern Shaanxi Loess Plateau, China. Journal of Arid Environments, 72(6), 974-985.

Liakatas, A., 1994. Harmonic analysis and modelling of annual soil temperature variations. Mausam, 45(2), 121-128.

Lian, X., Piao, S., Chen, A., Huntingford, C., Fu, B., Li, L. Z., Huang, J., Sheffield, J., Berg, A. M., & Keenan, T. F., 2021. Multifaceted characteristics of dryland aridity changes in a warming world. Nature Reviews Earth & Environment, 2(4), 232-250.

Liu, Y., Yue, H., Li, Y., & Lu, Y., 2018. Remote Sensing Monitoring of Spring Drought in Henan Province Based on MODIS. Agric. Res. Arid(36), 218–223.

Mann, H. B., 1945. Nonparametric tests against trend. Econometrica: Journal of the econometric society, 245-259.

Martin-Sotoca, J. J., Sanz, E., Saa-Requejo, A., Moratiel, R., Almeida-Ñauñay, A. F., & Tarquis, A. M., 2023. Agronomic and edaphic drought relations. A semiarid rangeland case. Natural Hazards and Earth System Sciences Discussions, 2023, 1-25.

McEvoy, D. J., Huntington, J. L., Hobbins, M. T., Wood, A., Morton, C., Anderson, M., & Hain, C., 2016. The evaporative demand drought index. Part II: CONUS-wide assessment against common drought indicators. Journal of Hydrometeorology, 17(6), 1763-1779.

McKee, T. B., Doesken, N. J., & Kleist, J. (1993). The relationship of drought frequency and duration to time scales. Proceedings of the 8th Conference on Applied Climatology,

Meher-Homji, V., 1991. Probable impact of deforestation on hydrological processes. Climatic change, 19(1), 163-173.

Mishra, A. K., & Singh, V. P., 2010. A review of drought concepts. Journal of hydrology, 391(1-2), 202-216.

Mitchell Jr, J. M., 1966. Climatic change: report of a working group of the Commission for Climatology. (No Title).

Mitchell Jr, J. M., Stockton, C. W., & Meko, D. M. (1979). Evidence of a 22-year rhythm of drought in the western United States related to the Hale solar cycle since the 17th century. Solar-Terrestrial Influences on Weather and Climate: Proceedings of a Symposium/Workshop held at the Fawcett Center for Tomorrow, The Ohio State University, Columbus, Ohio, 24–28 August, 1978,

Modarres, R., & Ouarda, T. B., 2014. Modeling the relationship between climate oscillations and drought by a multivariate GARCH model. Water Resources Research, 50(1), 601-618.

Mokarram, M., & Zarei, A. R., 2023. Soil erosion prediction using Markov and CA-Markov chains methods and remote sensing drought indicators. Ecological Informatics, 78, 102386.

Moran, M., Clarke, T., Inoue, Y., & Vidal, A., 1994. Estimating crop water deficit using the relation between surface-air temperature and spectral vegetation index. Remote Sensing of environment, 49(3), 246-263.

Morris, M. E., 1997. Water and conflict in the Middle East: Threats and opportunities. Studies in conflict & terrorism, 20(1), 1-13.

Narasimhan, B., & Srinivasan, R., 2005. Development and evaluation of Soil Moisture Deficit Index (SMDI) and Evapotranspiration Deficit Index (ETDI) for agricultural drought monitoring. Agricultural and Forest Meteorology, 133(1-4), 69-88.

Niedźwiedź, T., Twardosz, R., & Walanus, A., 2009. Long-term variability of precipitation series in east central Europe in relation to circulation patterns. Theoretical and Applied Climatology, 98, 337-350.

Niranjan Kumar, K., & Ouarda, T., 2014. Precipitation variability over UAE and global SST teleconnections. Journal of geophysical research: atmospheres, 119(17), 10,313-310,322.

Niranjan Kumar, K., Ouarda, T. B., Sandeep, S., & Ajayamohan, R. S., 2016. Wintertime precipitation variability over the Arabian Peninsula and its relationship with ENSO in the CAM4 simulations. Climate dynamics, 47, 2443-2454.

Oki, T., & Kanae, S., 2006. Global hydrological cycles and world water resources. science, 313(5790), 1068-1072.

Otkin, J. A., Anderson, M. C., Hain, C., Mladenova, I. E., Basara, J. B., & Svoboda, M., 2013. Examining rapid onset drought development using the thermal infrared–based evaporative stress index. Journal of Hydrometeorology, 14(4), 1057-1074.

Ouarda, T. B., Charron, C., Kumar, K. N., Marpu, P. R., Ghedira, H., Molini, A., & Khayal, I., 2014. Evolution of the rainfall regime in the United Arab Emirates. Journal of Hydrology, 514, 258-270.

Ouarda, T. B., Charron, C., Mahdi, S., & Yousef, L. A., 2021. Climate teleconnections, interannual variability, and evolution of the rainfall regime in a tropical Caribbean island: case study of Barbados. Theoretical and Applied Climatology, 145, 619-638.

Ouarda, T. B., Yousef, L. A., & Charron, C., 2019. Non-stationary Intensity-Duration-Frequency curves integrating information concerning teleconnections and climate change. International journal of climatology, 39(4), 2306-2323.

Ozelkan, E., Chen, G., & Ustundag, B. B., 2016. Multiscale object-based drought monitoring and comparison in rainfed and irrigated agriculture from Landsat 8 OLI imagery. International Journal of Applied Earth Observation and Geoinformation, 44, 159-170.

Palmer, W. C., 1968. Keeping track of crop moisture conditions, nationwide: the new crop moisture index.

Páscoa, P., Gouveia, C. M., Russo, A. C., Bojariu, R., Vicente-Serrano, S. M., & Trigo, R. M., 2020. Drought impacts on vegetation in southeastern Europe. Remote Sensing, 12(13), 2156.

Piao, S., Ciais, P., Huang, Y., Shen, Z., Peng, S., Li, J., Zhou, L., Liu, H., Ma, Y., & Ding, Y., 2010. The impacts of climate change on water resources and agriculture in China. Nature, 467(7311), 43-51.

Puletti, N., Mattioli, W., Bussotti, F., & Pollastrini, M., 2019. Monitoring the effects of extreme drought events on forest health by Sentinel-2 imagery. Journal of Applied Remote Sensing, 13(2), 020501-020501.

Raczyński, K., & Dyer, J., 2023. Harmonic oscillator seasonal trend (HOST) model for hydrological drought pattern identification and analysis. Journal of Hydrology, 620, 129514.

Rodriguez, R., Llasat, M. C., & Rojas, E., 1994. Evaluation of climatic change through harmonic analysis. Recent Studies in Geophysical Hazards, 5-16.

Rouault, M., Roy, S. S., & Balling Jr, R. C., 2013. The diurnal cycle of rainfall in South Africa in the austral summer. International journal of climatology, 33(3), 770-777.

Sahour, H., Vazifedan, M., & Alshehri, F., 2020. Aridity trends in the Middle East and adjacent areas. Theoretical and Applied Climatology, 142, 1039-1054.

Sandholt, I., Rasmussen, K., & Andersen, J., 2002. A simple interpretation of the surface temperature/vegetation index space for assessment of surface moisture status. Remote sensing of environment, 79(2-3), 213-224.

Savtchenko, A., Ouzounov, D., Ahmad, S., Acker, J., Leptoukh, G., Koziana, J., & Nickless, D., 2004. Terra and Aqua MODIS products available from NASA GES DAAC. Advances in Space Research, 34(4), 710-714.

Schickedanz, P. T., & Bowen, E., 1977. The computation of climatological power spectra. Journal of Applied Meteorology and Climatology, 16(4), 359-367.

Schnur, M. T., Xie, H., & Wang, X., 2010. Estimating root zone soil moisture at distant sites using MODIS NDVI and EVI in a semi-arid region of southwestern USA. Ecological Informatics, 5(5), 400-409.

Selvam, A. M., & Joshi, R., 1995. Universal spectrum for interannual variability in COADS global air and sea-surface temperatures. International journal of climatology, 15(6), 613-623.

Sen, P. K., 1968. Estimates of the regression coefficient based on Kendall's tau. Journal of the American statistical association, 63(324), 1379-1389.

Shawky, M., Ahmed, M. R., Ghaderpour, E., Gupta, A., Achari, G., Dewan, A., & Hassan, Q. K., 2023. Remote sensing-derived land surface temperature trends over South Asia. Ecological Informatics, 74, 101969.

Shetty, S., 2006. Water, food security and agricultural policy in the Middle East and North Africa region.
Shoshany, M., & Mozhaeva, S., 2023. Climate and aridity measures relationships with spectral vegetation indices across desert fringe shrublands in the South-Eastern Mediterranean Basin. Environmental Monitoring and Assessment, 195(5), 563.
Sneyers, R. (1990). On the Statistical Analysis of Series of Observations, WMO Technical note, vol. 143. Secretariat of the World Meteorological Organization, ISBN 9789263104151. In.
Soltani, S., Saboohi, R., & Yaghmaei, L., 2012. Rainfall and rainy days trend in Iran. Climatic Change, 110, 187-213.
Son, N. T., Chen, C., Chen, C., Chang, L., & Minh, V. Q., 2012. Monitoring agricultural drought in the Lower Mekong Basin using MODIS NDVI and land surface temperature data. International Journal of Applied Earth Observation and Geoinformation, 18, 417-427.
Sun, L., Sun, R., Li, X., Liang, S., & Zhang, R., 2012. Monitoring surface soil moisture status based on remotely sensed surface temperature and vegetation index information. Agricultural and Forest Meteorology, 166, 175-187.
Sun, W., Wang, P. X., Zhang, S. Y., Zhu, D. H., Liu, J. M., Chen, J. H., & Yang, H. S., 2008. Using the vegetation temperature condition index for time series drought occurrence monitoring in the Guanzhong Plain, PR China. International journal of remote sensing, 29(17-18), 5133-5144.
Tagesson, T., Horion, S., Nieto, H., Fornies, V. Z., González, G. M., Bulgin, C., Ghent, D., & Fensholt, R., 2018. Disaggregation of SMOS soil moisture over West Africa using the Temperature and Vegetation Dryness Index based on SEVIRI land surface parameters. Remote Sensing of Environment, 206, 424-441.
Tang, R., Li, Z.-L., & Tang, B., 2010. An application of the Ts–VI triangle method with enhanced edges determination for evapotranspiration estimation from MODIS data in arid and semi-arid regions: Implementation and validation. Remote Sensing of Environment, 114(3), 540-551.
Tarawneh, Q., & Kadıoğlu, M., 2003. An analysis of precipitation climatology in Jordan. Theoretical and Applied Climatology, 74, 123-136.
Tase, N. (1976). *Area-deficit-intensity characteristics of droughts* Colorado State University. Libraries].
Tayanç, M., İm, U., Doğruel, M., & Karaca, M., 2009. Climate change in Turkey for the last half century. Climatic Change, 94(3-4), 483-502.
Torres, S. M., & Warde, D. A., 2017. Staggered-PRT sequences for Doppler weather radars. Part I: Spectral analysis using the autocorrelation spectral density. Journal of Atmospheric and Oceanic Technology, 34(1), 51-63.
Trenberth, K. E., Dai, A., Van Der Schrier, G., Jones, P. D., Barichivich, J., Briffa, K. R., & Sheffield, J., 2014. Global warming and changes in drought. Nature Climate Change, 4(1), 17-22.
Tsakiris, G., Pangalou, D., & Vangelis, H., 2007. Regional drought assessment based on the Reconnaissance Drought Index (RDI). Water resources management, 21, 821-833.
UNESCO. 2021. The United Nations World Water Development Report 2021: Valuing Water. United Nations.
Vicente-Serrano, S. M., Beguería, S., & López-Moreno, J. I., 2010. A multiscalar drought index sensitive to global warming: the standardized precipitation evapotranspiration index. Journal of climate, 23(7), 1696-1718.
Vicente-Serrano, S. M., Beguería, S., Lorenzo-Lacruz, J., Camarero, J. J., López-Moreno, J. I., Azorin-Molina, C., Revuelto, J., Morán-Tejeda, E., & Sanchez-Lorenzo, A., 2012. Performance of drought indices for ecological, agricultural, and hydrological applications. Earth Interactions, 16(10), 1-27.
Wan, W., Han, Y., Wu, H., Liu, F., Liu, Z., & . . 2021, 106910. 2021. Application of the source–sink landscape method in the evaluation of agricultural non-point.

source pollution: First estimation of an orchard-dominated area in China. Agric. Water Manag, 252, 106910.
Wan, Z., Wang, P., & Li, X., 2004. Using MODIS land surface temperature and normalized difference vegetation index products for monitoring drought in the southern Great Plains, USA. International journal of remote sensing, 25(1), 61-72.

Wang, H., Li, X., Long, H., Xu, X., & Bao, Y., 2010. Monitoring the effects of land use and cover type changes on soil moisture using remote-sensing data: A case study in China's Yongding River basin. Catena, 82(3), 135-145.

Wang, K., Li, Y., Luo, Z., Yin, S., & Chan, P. W., 2018. Harmonic analysis of 130-year hourly air temperature in Hong Kong: detecting urban warming from the perspective of annual and daily cycles. Climate Dynamics, 51, 613-625.

Wei, W., Pang, S., Wang, X., Zhou, L., Xie, B., Zhou, J., & Li, C., 2020. Temperature vegetation precipitation dryness index (TVPDI)-based dryness-wetness monitoring in China. Remote Sensing of environment, 248, 111957.

Wei, W., Zhang, J., Zhou, L., Xie, B., Zhou, J., & Li, C., 2021. Comparative evaluation of drought indices for monitoring drought based on remote sensing data. Environmental Science and Pollution Research, 28, 20408-20425.

World Health Organization. 2019. The state of food security and nutrition in the world 2019: safeguarding against economic slowdowns and downturns (Vol. 2019). Food & Agriculture Org.

Wu, D., Qu, J. J., & Hao, X., 2015. Agricultural drought monitoring using MODIS-based drought indices over the USA Corn Belt. International Journal of Remote Sensing, 36(21), 5403-5425.

Yilmaz, B., 2019. Analysis of hydrological drought trends in the gap region (southeastern turkey) by mann-kendall test and innovative şen method. Applied Ecology & Environmental Research, 17(2).

Yu, Y.-S., Zou, S., & Whittemore, D., 1993. Non-parametric trend analysis of water quality data of rivers in Kansas. Journal of hydrology, 150(1), 61-80.

Yuan, X., Wang, L., Wu, P., Ji, P., Sheffield, J., & Zhang, M., 2019. Anthropogenic shift towards higher risk of flash drought over China. Nature communications, 10(1), 4661.

Zeleke, T. T., Giorgi, F., Diro, G., & Zaitchik, B., 2017. Trend and periodicity of drought over Ethiopia. International journal of climatology, 37(13), 4733-4748.

Zhai, L., & Feng, Q., 2009. Spatial and temporal pattern of precipitation and drought in Gansu Province, Northwest China. Natural Hazards, 49, 1-24.

Zhang, W., An, S., Xu, Z., Cui, J., & Xu, Q., 2011. The impact of vegetation and soil on runoff regulation in headwater streams on the east Qinghai–Tibet Plateau, China. Catena, 87(2), 182-189.

Zhu, X., Li, Q., & Guo, C., 2024. Evaluation of the monitoring capability of various vegetation indices and mainstream satellite band settings for grassland drought. Ecological Informatics, 82, 102717.

Zormand, S., Jafari, R., & Koupaei, S. S., 2017. Assessment of PDI, MPDI and TVDI drought indices derived from MODIS Aqua/Terra Level 1B data in natural lands. Natural Hazards, 86, 757-777.

Highlights

- Significant seasonal TVDI trends: upward in northern, downward in southern Middle East.
- Seasons show varied TVDI trends: steep spring ups, notable summer downs.
- Annual TVDI trend map shows long-term decline, especially below 34 degrees latitude.
- Periodograms reveal cyclic TVDI patterns linked to ENSO and atmospheric factors.